Permian tectonic evolution of proto-Japan: Insights from detrital zircon geochronology and crystal morphology

（ペルム紀原日本の構造進化：砕屑性ジルコン年代及び形態からの洞察）

Masahiro Ohkawa

（大川　真弘）

A dissertation for the degree of Doctor of Science

Department of Earth and Environmental Sciences,

Graduate School of Environmental Studies, Nagoya University

（名古屋大学大学院環境学研究科地球環境科学専攻　学位論文 博士（理学））

2023

Content:

Abstract

Japan has evolved along the Paleo-Pacific Ocean as an arc–trench system in the Phanerozoic. However, the relationship between Japan and the older continental crust such as Sino–Korean and South China Blocks is unclear. This study compared published and new measured data of detrital zircon ages and morphology from Permian fore-arc accretionary complexes (Akiyoshi Belt) and back-arc basin deposits (Maizuru Belt) in Japan. The fore- and a part of back-arc deposits consist mainly of the late Paleozoic zircon grains that are close to the depositional ages and generally angular to subangular. These grains were supplied mainly from a volcanic arc isolated from the older continental crust, and the source rocks were exposed immediately prior to their erosion and transport and transported directly to the depositional site in a relatively short time. On the other hand, a part of back-arc deposits generally contains Precambrian to Paleozoic zircon grains that are commonly older than their depositional ages and rounded. These grains were supplied from multiple sources such as the volcanic arc and Precambrian continental block and were affected by long-distance transport and/or strong hydrodynamics in the marine environment during transport. Moreover, comprehensive detrital zircon data in the fore- and back-arc deposits emphasize that the island arc–back-arc basin–continental margin system has been formed along the eastern margin of East Asia, and the volcanic arc collided with the eastern margin of Sino–Korean Block during the Permian. The detritus derived from the continental crust were captured by a back-arc basin and blocked by the uplift zone of the volcanic arc. However, a small amount of detritus originating from the continental crust were supplied to the fore-arc.

1. Introduction

Proto-Japan, the source of present-day Japan, was born as a part of a passive continental margin due to the late Neoproterozoic breakup of the supercontinent Rodinia (Isozaki et al., 2010, 2015). In the proto-Japan, the arc–trench system along the Paleo-Pacific Ocean developed by the Cambrian (Isozaki et al., 2015; Yamazaki, 2020) and grew throughout the Phanerozoic forming active subduction zones (Isozaki et al., 2010; Isozaki, 2019). de Jong et al. (2009) called the Permian igneous rocks such as those of the Paleo-Ryoke Belt, and older subduction–accretion complexes, which are presently dispersed in the Japanese islands the proto-Japan. The proto-Japan has undergone multiple tectonic movements (e.g., collision and strike-slip movements) since the Paleozoic (e.g., Faure and Charvet, 1987; Faure and Natal'in, 1992; Hada et al., 2001; Taira, 2001; de Jong et al., 2009; Isozaki et al., 2010; Suda et al., 2014; Ohkawa et al., 2022). Among these events, the cause of late Paleozoic collisional orogenesis is

not clear owing to the scarcity of geological information (especially igneous and metamorphic rocks). Many researchers considered that the collisional belt between the Sino–Korean and South China Blocks extended to the Japanese region (e.g., Ishiwatari and Tsujimori, 2003; Osanai et al., 2006; Tsujimori et al., 2006; Ernst et al. 2007; Oh and Kusky, 2007). On the other hand, de Jong et al. (2009) concluded that the proto-Japan collided with the eastern margin of Sino–Korean Block during the late Paleozoic to early Mesozoic. In contrast to the sporadic distribution of late Paleozoic igneous and metamorphic rocks, non-metamorphic sedimentary rocks are widely distributed in Northeast and Southwest Japan (Fig. 1). Therefore, those provenance analyses are considered to be a key to understanding the tectonic evolution of proto-Japan and East Asia.

U–Pb dating of detrital zircon is possible to identify the age of the source (e.g., Gehrels, 2014), constrain the depositional environments based on age spectra reflected by the tectonic setting of the depositional basin (Cawood et al., 2012), and define the maximum depositional age (e.g., Dickinson and Gehrels, 2009). Therefore, it is used extensively for provenance analysis of sediments (e.g., Fildani et al., 2003; Yue et al., 2005; Cawood et al., 2012; Yao et al., 2014; Tokiwa et al., 2019; Wen et al., 2021), and several studies were conducted on the provenance analysis of Permian sedimentary rocks in Japan (e.g., Okawa et al., 2013; Hara et al., 2018; Zhang et al., 2018a; Ohkawa et al., 2021, 2022; Pastor-Galán et al., 2021; Suzuki and Kurihara, 2021; Li and Takeuchi, 2022). However, these depositional environments, tectonic evolution, and transport processes from the source have not been understood well enough. Permian non-metamorphosed sedimentary rocks are divided into fore-arc shelf (South Kitakami, Hida-Gaien, and a part of Kurosegawa Belts), basin and/or slope basin deposits (a part of Akiyoshi Belt), accretionary complexes (Ultra-Tamba and a part of Akiyoshi and Kurosegawa Belts) and back-arc basin deposits (Maizuru Belt) (e.g., Takeuchi et al., 2008; Wakita et al., 2018) in Japan (Fig. 2). Therefore, a comprehensive examination of Permian fore-arc and back-arc provenance can provide a constraint on the tectonic evolution of proto-Japan and East Asia.

Two major processes control the shape parameters of detrital zircon grain: (1) zircon growth mechanisms in the magmatic host rocks, (2) hydrothermal and metamorphic processes after zircon formation and exogenous processes such as chemical and mechanical weathering and sediment transport (Zeh and Cabral, 2021). Among these, rounded grains derived from the host rocks and/or affected by some physicochemical processes (e.g., recrystallization, corrosion, and chemical erosion) are rarely contained in the sediments (Gärtner et al., 2013; Zeh and Cabral, 2021 and references therein). On the other hand, the relationship between the zircon

shape and transport process is still being discussed (e.g., Gärtner et al., 2013; Garzanti et al., 2015; Zoleikhaei et al., 2016; Markwitz et al., 2017; Sundell et al., 2018). However, several studies have reported that the shape is affected by transport distance and hydrodynamic process during transport (e.g., Gärtner et al., 2017; Markwitz et al., 2017; Sundell et al., 2018; Zeh and Cabral, 2021; Zeh and Wilson, 2022). Moreover, the shape of zircon provides additional information about the host rock (e.g., Pupin, 1980; Tietz et al., 2003; Belousova et al., 2006; Gärtner et al., 2017; Zieger et al., 2019). Therefore, shape parameters such as length, width, elongation, and morphology of zircons can constrain the depositional environments, transport processes, and source rocks.

In order to solve issues related to the tectonic evolution of East Asia and proto-Japan, we investigated U–Pb ages and crystal morphology of detrital zircons from the Permian fore-arc deposits (Akiyoshi Belt) and compared them with those of the Permian back-arc deposits (Maizuru Belt) measured by Ohkawa et al. (2022) (Table 1). The middle to late Permian sediments of the Akiyoshi and Maizuru Belts were deposited at the same latitude by the similarity of the brachiopod faunas (Tazawa et al., 2009 and references therein). Furthermore, the Permian detritus of the Akiyoshi and Maizuru Belts is suggested to have a common provenance based on the studies of conglomerates and detrital heavy minerals (Kano, 1961; Kano et al., 1961; Takeuchi et al., 2008). Therefore, provenance analysis of the Akiyoshi and Maizuru Belts can discuss the relationship between the fore- and back-arc deposits of proto-Japan, and the variation of their depositional environment and tectonics. Moreover, this study quantitatively evaluated the dissimilarity of U–Pb age data of detrital zircons from the Akiyoshi and Maizuru Belts (Zhang et al., 2018a; Kimura et al., 2021; Ohkawa et al., 2022; this study) by using a multidimensional scaling (MDS) method. The MDS is a helpful tool for visualizing the dissimilarity of a large dataset and is widely used for provenance analysis using detrital zircons (e.g., Vermeesch, 2013; Ortega-Flores et al., 2021; Pastor-Galán et al., 2021; Ma et al., 2022; Malkowski et al., 2022). Based on a combined method of detrital zircon geochronology and crystal morphology from fore- and back-arc deposits, we discuss the Permian tectonic evolution of proto-Japan and the relationship with East Asian continental blocks, while considering the differences in their depositional environments.

2. Geological setting

The Japanese archipelago is divided into Northeast and Southwest Japan by the Tanakura Tectonic Line, and Southwest Japan is subdivided into Inner and Outer zones by the Median Tectonic Line (e.g., Ichikawa, 1990; Takagi and Arai, 2003; Takeuchi et al., 2008; Pastor-Galán

3

et al., 2021) (Fig. 1). The Akiyoshi Belt is sparsely distributed in the Inner Zone of Southwest Japan (Fig. 1), and consist mainly of a late Paleozoic accretionary complex that contains sandstone, mudstone, chert, limestone, and basalt (Kanmera and Nishi, 1983; Sano and Kanmera, 1988). There are several studies examining the provenance, depositional and tectonic environments of their sediments (e.g., Sano and Kanmera, 1988; Hara and Kiminami, 1989; Takeuchi et al., 2008; Zhang et al., 2018a). The carbonates of Akiyoshi Belt were deposited in an open-ocean seamount of the Paleo-Pacific Ocean (Panthalassan Ocean) by stratigraphy, paleontology, and sedimentology (e.g., Sano and Kanmera, 1988; Nakazawa, 2001). Based on stratigraphical and sedimentological studies, the detrital rocks were deposited mainly in a trench and trench-slope basin around the convergent margin (Tanaka et al., 1987; Hara and Kiminami, 1989; Matsuzawa and Takeuchi, 2009) and partly in fore-arc basin (Wakita et al., 2018). Based on compositions of sandstones and detrital heavy minerals, it is suggested that the provenance of the Akiyoshi Belt contained a volcanic arc containing calcareous metamorphic rocks, and the detritus was supplied by progressive uplifting and denudation of the volcanic arc (Takeuchi et al., 2008; Zhang et al., 2018a). Moreover, Takeuchi et al. (2008) reported that its provenance contained igneous rocks of the Maizuru Belt based on the chemical compositions of detrital chromian spinels. On the other hand, there are some opinions on the relationship between the continental crust of East Asia and Akiyoshi Belt (e.g., Tsutsumi et al., 2000; Takeuchi et al., 2008; Nakama et al., 2010; Zhang et al., 2018a, 2019).

In the Itoigawa area of Niigata Prefecture, the Akiyoshi Belt consists of Omi Complex (Carboniferous to Permian sedimentary succession) and Himekawa Complex (middle Permian sedimentary succession) (Fig. 3). The Omi Complex is composed of limestone and basalt, and the Himekawa Complex is composed of chert, felsic tuff, mudstone, sandstone, and conglomerate (Takeuchi et al., 2008; Nagamori et al., 2010). The middle Permian sedimentary succession is subdivided into the Eastern, Central, and Western Units by stratigraphy and geological structure (Fig. 3). The Western Unit consists of reddish-brown siliceous mudstone, red chert, alternating beds of felsic tuff and black mudstone, mudstone, and sandstone with mudstone and conglomerate in ascending stratigraphic order (Fig. 4 Route A). The stratigraphy of the Eastern and Central Units is similar, and they consist mainly of mudstone, thin bedded sandstone, and massive sandstone in ascending stratigraphic order (Fig. 4 Route B, C, D). The succession is more than 600 m thick (Takeuchi et al., 2008; Nagamori et al., 2010), and middle Permian radiolarian assemblages of *Pseudoalbaillella longtanensis–Follicucullus monacanthus* zones (Ishiga, 1986, 1990) were found in the chert, siliceous mudstone, and manganese carbonate (Tazawa et al., 1984, Ujihara, 1985, Kawai and Takeuchi, 2001). The

Central Unit is structurally overlain by the Eastern Unit, and the Eastern and Central Units are separated from the Western Unit by high-angle faults. The succession is in contact with the Maizuru Belt by high-angle faults (Nagamori et al., 2010) (Fig. 3).

The Maizuru Belt is sporadically distributed in the Inner zone of Southwest Japan and is in contact with the Akiyoshi, Suo, and Ultra-Tamba Belts (Fig. 1). It is subdivided into Southern, Central, and Northern zones based on lithology and geological structure (Kano et al., 1959). The Southern zone consists mainly of Yakuno ophiolite (ultramafic and mafic rocks) with granitic and metamorphic rocks (Hayasaka et al., 1996; Ichiyama and Ishiwatari, 2004; Suda and Hayasaka, 2009). The Central zone is composed of Permian to Triassic sediments (Nakazawa, 1957; Shimizu, 1962a; Hayasaka, 1990), and the lower part of Permian sedimentary succession is accompanied by back-arc basin basalts (Koide, 1986; Koide et al., 1987). The Northern zone consists mainly of granitic rock with metamorphic rock, dolerite, and gabbro (Igi et al., 1961; Igi and Kuroda, 1965; Hayasaka et al., 1996; Fujii et al., 2008). The Permian to Triassic sedimentary successions in the Central Maizuru Belt confirmed changes of the depositional environment (Shimizu, 1962b; Shiki, 1962; Mavoungou et al., 2022). In the early depositional stage of the Permian sedimentary succession, the succession is considered to be deposited in a quiet shallow sea (Shimizu et al., 1962b). On the other hand, gravity flow and terrestrial deposits were deposited in the late stage of the Permian sedimentary succession (Shimizu, 1962a; Suzuki, 1987; Mavoungou et al., 2022). The Late Triassic sedimentary succession of the Maizuru Belt contained molasse-type deposits (Shiki, 1962). Based on the lithology and geochronology of the conglomerate, it is suggested that the provenance had the rocks of Southern and Northern Maizuru Belts (Kano, 1961; Kano et al., 1961; Mavoungou et al., 2022). The relationship between the Maizuru Belt and older continental crust is not clear the same as the Akiyoshi Belt (e.g., Kobayashi, 2003; Nakama et al., 2010; Tsutsumi et al., 2014; Kimura et al., 2019, 2021; Ohkawa et al., 2022).

In the Itoigawa area of Niigata Prefecture, the Maizuru Belt is composed of Mushikawa Formation (middle Permian sedimentary succession), Kotozawa Igneous Rocks (igneous rock with metamorphic rock), and Kuratani Metamorphic Rocks (metamorphic rock with igneous rock) (Nagamori et al., 2010). The sedimentary succession is subdivided into lower (mudstone with sandstone) and upper parts (breccia with mudstone and sandstone) and is more than 600 m thick. The sandstones of the succession are white, gray, or gray-green lithic sandstones (Nagamori et al., 2010; Ohkawa et al., 2022). The breccias contain fragments of various sizes (several millimeters to 5 cm) such as basalt, dolerite, gabbro, mudstone, sandstone, chert, felsic volcanics, granitoids, tuff, and crystalline schist (Nagamori et al., 2010) (Fig. 4). Middle

Permian radiolarian assemblages of *Pseudoalbaillella longtanensis–Pseudoalbaillella globosa* zones (Ishiga, 1986, 1990) were found in the mudstones (Ujihara, 1985; Kawai and Takeuchi, 2001). By the lithology and radiolarian assemblages, the succession is correlated with the lower to middle parts of the Permian sedimentary succession (Maizuru Group) in the Central Maizuru Belt (Kawai and Takeuchi, 2001). U–Pb ages of 415 ± 8.1, 393 ± 11, 389 ± 8.4, 381 ± 24, 330 ± 12, and 310 ± 12 Ma were reported from mafic blocks of the succession (Koshiba et al., 2018). The succession is in contact with the Kotozawa Igneous Rocks and Kuratani Metamorphic Rocks by high-angle faults (Nagamori et al., 2010). The Kotozawa Igneous Rocks consist of basalt, dolerite, gabbro, and metagabbro (Nagamori et al., 2010), and U–Pb zircon age of 416 ± 9.3 Ma were reported from the gabbro (Suda et al., 2010). The Kuratani Metamorphic Rocks is composed of gabbro, tonalite, quartz diorite, and schist (Nagamori et al., 2010).

3.   Sample collection

The Western Unit, the middle Permian sedimentary succession of Akiyoshi Belt, confirmed chert-clastic sequences from chert to coarse-grained clastic rock (Fig. 4). The Eastern Unit lacks the chert and siliceous mudstone, although its area accounts for a large part of the sedimentary successions. Moreover, Takeuchi et al. (2008) reported changes of the sandstone compositions of the Eastern Unit. Because the Western and Eastern Units have been investigated in their stratigraphy by several researchers in detail (Takeuchi et al., 2008; Matsuzawa and Takeuchi, 2009), we collected 23 sandstone samples from the Western and Eastern Units and analyzed modal composition. Moreover, analyses of U−Pb age and crystal morphology of detrital zircons were conducted from 8 sandstone samples (Fig. 4 and Table 1).

This study compares detrital zircon morphology and age data from the middle Permian sedimentary succession of the Maizuru Belt by Ohkawa et al. (2022) with those of the Akiyoshi Belt due to discuss the tectonic evolution of the Permian proto-Japan. Furthermore, the depositional environment and provenance changes were analyzed by combining the detrital zircon and sandstone composition data by this and previous studies (Kimura et al., 1988; Kusunoki and Musashino, 1990; Suzuki, 1992; Zhang et al., 2018a; Kimura et al., 2021).

4.   Methods
4.1.   Sandstone petrography

The modal compositions of the sandstone samples were measured by point counting in the thin sections. We counted by the traditional QFR method (R means rock fragments) and the

Gazzi–Dickinson QFL method (Dickinson, 1970; Ingersoll et al., 1984), and 499 to 619 points were counted in each thin section. They are poorly sorted, angular to subangular, and medium to coarse-grained sandstones (Fig. 5). The K-feldspars were stained for their clear identification based on a method of Bailey and Stevens (1960). The results were plotted by using the Qm–F–Lt (Dickinson, 1985), Q–F–R (Folk, 1968, 1980), and Lm–Lv–Ls (Ingersoll and Suczek, 1979) triangular diagrams (Fig. 6).

4.2. Detrital zircon morphology and U−Pb geochronology

Based on the process of Ohkawa et al. (2022), the samples were crushed by a jaw crusher and stamp mill and subsampled to a 60 mesh (250 μm) sieve. Then, heavy-mineral concentrates were obtained by water panning, and magnetic minerals were removed by a magnet. Zircon grains were arrayed onto microscope slides, and secondary electron images were acquired with a Hitachi S-3400N scanning electron microscope (SEM) at the Nagoya University Museum (Fig. 6). In order to avoid sampling bias, zircons were picked exhaustively by hand under a stereoscope, independent of shape, color, or crack. The shape (length, width, elongation, and roundness) and morphotype of the zircon were obtained under the stereoscope and SEM (Figs. 8 and 9 and Table 2). The classification of shape (roundness and elongation) and morphotype followed the methods of Gärtner et al. (2013) and Pupin (1980), respectively.

After observation, the zircons were mounted onto an epoxy resin-coated microscope slide, and cathodoluminescence images were acquired with by a Hitachi S-3400N SEM with a GATAN MiniCL at the Nagoya University Museum based on the processes of Ohkawa et al. (2021, 2022) (Fig. 6). U–Pb age dating of zircons was performed with an Agilent 7700 inductively coupled plasma–mass spectrometer and an Elemental Scientific Laser NWR213 Nd:YAG ($\lambda = 213$ nm) laser ablation system at the Graduate School of Environmental Studies, Nagoya University. Analyses were conducted under the following conditions: energy density of 11.7 J/cm^2, pulse repetition rate of 10 Hz, and crater diameter of 25 μm (Kouchi et al., 2015). U–Pb ratio was normalized by the 91500 zircon standard (1062.4 ± 0.4 Ma; Wiedenbeck et al., 1995) and Plešovice zircon standard (337.13 ± 0.37 Ma; Sláma et al., 2008) was simultaneously analyzed as quality control.

The filtering process of analysis results using ratios of disagreement from two or more isotopic systems provides a qualitative assessment of whether the U–Pb isotopic system experienced disturbances (e.g., Gehrels, 2014; Spencer et al., 2016). Because discordance in the system cannot be ignored radiogenic lead loss or other isotopic disturbances, zircons within 90–110 % of the concordance ratio were adopted for discussion (e.g., Belousova et al., 2009;

Wang et al., 2014; Spencer et al., 2016; Ohkawa et al., 2021, 2022). The following formula computed the concordance ratio (Conc.): Conc. (%) = [1 − (^{206}Pb/^{238}U age)/(^{207}Pb/^{235}U age)] × 100 (Hidaka et al., 2002). ^{207}Pb/^{206}Pb age for zircon was adopted older than 1.2 Ga, whereas ^{206}Pb/^{238}U age for that younger was used (Gehrels et al., 2008). The age distribution was plotted by using detzrcr package (Andersen et al., 2018) of R software (R Core Team, 2021) (Fig. 10). Moreover, we discussed the relationship among the age, Th/U ratio, and morphology (Figs. 11–14).

The cumulative distribution plot showing the gap between the crystallization and depositional ages can provide insights into the source of zircon and the tectonic setting of the sedimentary basin (Cawood et al., 2012) (Fig. 14). Therefore, the detrital zircon age spectra for the Akiyoshi and Maizuru Belts were plotted as the cumulative distribution functions. Cawood et al. (2012) reported that age distribution patterns from detrital zircons principally controlled by the volumes of magma generated in each tectonic setting and their preservation potential, and they could be grouped into three main tectonic settings of convergent, collisional, and extensional. Furthermore, multidimensional scaling (MDS) maps (Vermeesch, 2013) of detrital zircon age data for the Akiyoshi and Maizuru Belts were created using DZmds (Saylor et al., 2018) of MATLAB algorithm. MDS is a useful tool for visualizing the dissimilarities of a multivariate dataset with distance, in which clustered samples are more similar, whereas spread samples are not similar (Vermeesch, 2013). This study calculated the sample dissimilarity by using the Kuiper V value (e.g., Ma et al., 2022; Malkowski et al., 2022) (Fig. 14). The closest and second-closest neighbors in the MDS map were indicated by solid and dashed lines, respectively. The suitability of the MDS map was confirmed by a Shepard plot (Fig. 14), and it is indicated by the stress value of the MDS configurations (0.20 = poor; 0.10 = fair; 0.05 = good) (Vermeesch, 2013). The stress values (0.061402) reflect a relatively good fit, suggesting the MDS plot is meaningful (Fig. 14).

5. Analysis results

5.1. Sandstone petrography

Photomicrographs and modal compositions from sandstone samples are shown in Figs. 5 and 6, respectively.

5.1.1. Fore-arc deposits (Akiyoshi Belt)

The sandstones of the middle Permian sedimentary succession of the Akiyoshi Belt were the following two types: feldspathic and lithic arenites (Takeuchi et al., 2008). The sandstones of

the Western Unit were feldspathic arenite, whereas those of the Eastern Unit changed from lithic to feldspathic arenite in ascending stratigraphic order (Takeuchi et al., 2008).

Based on the Q–F–R plot, the samples of the Western Unit were classified into lithic arkose (A2 to A9) and feldspathic litharenite (A11). They were plotted at the magmatic arc provenance field (dissected and transitional arcs) based on the Qm–F–Lt plot (Fig. 6). The average composition of the sandstones in the Western Unit is $Qm_{25.0}$ $F_{41.8}$ $Lt_{33.2}$ and $Q_{27.3}$ $F_{41.3}$ $R_{31.4}$. The sandstones consisted mainly of quartz and plagioclase, and rare K-feldspar, biotite, calcite, chlorite, epidote, muscovite, titanite, and zircon (Fig. 5). The quartz grains were mainly monocrystalline (18–29 %) and few polycrystalline (1-5 %). Some grains showed weak wavy extinction and partial corrosion. The number of plagioclase grains (20–30 %) was more than those of K-feldspar (7–17 %), and some plagioclase displayed saussuritization or sericitic alteration. They contained fragments of abundant volcanic rock (73–92 % of the total rock fragments) and rare sedimentary (7–27 %) and metamorphic rocks (0–2 %) and distributed mainly in the magmatic arc field based on the Lm–Lv–Ls plot (Fig. 6). They contained fragments of abundant felsic volcanics and tuff with andesite, basalt, granite, granophyre, mica schist, quartz schist, hornfels, mudstone, chert, and limestone.

The samples of the Eastern Unit were classified into lithic arkose (B7–10 and C1–3), feldspathic litharenite (B0, 1, 2, 3, 5, 6), and litharenite (B4) based on the Q–F–R plot. They belonged to the magmatic arc provenance field (undissected, dissected, and transitional arcs) based on the Qm–F–Lt plot. Their feldspathic components of Route B increase upward, whereas those of Route C unalter (Fig. 6). The average compositions of Route B and C were $Qm_{22.3}$ $F_{35.7}$ $Lt_{42.0}$ and $Q_{24.9}$ $F_{34.3}$ $R_{40.8}$, and $Qm_{22.6}$ $F_{45.5}$ $Lt_{31.9}$ and $Q_{26.4}$ $F_{44.9}$ $R_{28.7}$, respectively. The sandstones were composed mainly of quartz and plagioclase with K-feldspar, biotite, calcite, chlorite, epidote, hornblende, muscovite, titanite, and zircon (Fig. 5). The quartz grains were mainly monocrystalline (13–23 %) and few polycrystalline (1-5 %), and a part of the grains showed weak wavy extinction and partial corrosion. The number of plagioclase grains (12–36 %) was more than K-feldspar (2–12 %), and some plagioclase displayed sericitic alteration or saussuritization. They contained fragments of abundant volcanic rock (82–99 % of the total rock fragments) and rare sedimentary (0–17 %) and metamorphic rocks (0–3 %) and distributed mainly in the magmatic arc field based on the Lm–Lv–Ls plot (Fig. 6). They contained fragments of abundant felsic to intermediate volcanics and tuff with basalt, granite, granophyre, mica schist, quartz schist, hornfels, mudstone, chert, and limestone (Fig. 5).

5.1.2. Back-arc deposits (Maizuru Belt)

Several researchers reported Permian to Triassic sandstone compositions of the Maizuru Belt (e.g., Kimura et al., 1988; Kusunoki and Musashino, 1990; Suzuki, 1992). Based on the Q–F–R plot, the Permian sandstones were classified into feldspathic litharenite and litharenite, and the Triassic sandstones were cataloged as feldspathic litharenite. The Permian sandstones were plotted at the lithic recycled and undissected and transitional arcs and the Early to Middle Triassic sandstones were plotted at the transitional recycled and transitional and dissected arcs. The Late Triassic sandstones belonged to the transitional arc and mixed fields (Fig. 6). Based on sandstone composition data of Kusunoki and Musashino (1990) and Suzuki (1992), the average compositions of the Permian, Early to Middle Triassic, and Late Triassic sandstones were $Qm_{8.6}$ $F_{22.6}$ $Lt_{68.8}$ and $Q_{9.1}$ $F_{18.2}$ $R_{72.7}$, $Qm_{29.4}$ $F_{26.4}$ $Lt_{44.2}$ and $Q_{38.9}$ $F_{25.1}$ $R_{36.0}$, and $Qm_{34.3}$ $F_{23.3}$ $Lt_{42.3}$ and $Q_{58.6}$ $F_{20.2}$ $R_{21.1}$, respectively. The quartz and feldspar components of the Permian to Triassic sandstones increased upward. In contrast, the ratios of their rock fragments decreased (Fig. 6). Moreover, the Permian sandstones consisted mainly of plagioclase (9-21 %) with rare K-feldspar (1–2%), whereas Triassic sandstones increased the number of K-feldspar and contained plagioclase of 7–21 % and K-feldspar of 4–17 % (Kusunoki and Musashino, 1990; Suzuki, 1992). They had fragments of abundant volcanic rock (>60 % of the total rock fragments), common sedimentary (ca. 10–30 %), and rare metamorphic rocks (Fig. 6). The rock fragments of the Permian to Middle Triassic sandstones were composed mainly of felsic to intermediate volcanics with mafic volcanics, sedimentary rocks (chert, mudstone, sandstone, and limestone), and metamorphic rocks (Kusunoki and Musashino, 1990; Suzuki, 1992; Ohkawa et al., 2022). On the other hand, rock fragments of the Late Triassic sandstones consisted mainly of granitic rocks (Kusunoki and Musashino, 1990).

5.2. Crystal morphology of the detrital zircons

The SEM and CL images of the detrital zircon are shown in Fig. 7, and the shapes (length, width, elongation, and roundness) are shown in Fig. 8 and Table 2. Moreover, the morphotypes are shown in Fig. 9.

5.2.1. Fore-arc deposits (Akiyoshi Belt)

In the middle Permian sedimentary succession of the Akiyoshi Belt, 8 sandstone samples yielded 699 concordant ages from total 1291 spots, and the morphotypes of 519 grains were classified (Fig. 9).

In the Western Unit, the lengths from samples A2 and A9 were 59–213 (mean: 98.6 μm) and

49–254 μm (mean: 97.7 μm), and their widths were 41–117 μm (mean: 69.0 μm) and 36–151 μm (mean: 68.5 μm), respectively (Fig. 8 and Table 2). The mean elongation values (width/length) from samples A2 and A9 were 0.72 (Fig. 8 and Table 2), which were categorized as "short-stubby" (Gärtner et al., 2013 and references therein). The mean roundness values from samples A2 and A9 were 4.0 and 3.8, respectively (Fig. 8 and Table 2), and they were usually euhedral, angular to subangular. Based on the morphotype classification (Pupin, 1980), S7, S19, S24, and G1–3 types accounted for more than 10% of the total grains, and S2, S12, and S17 types accounted for more than 5% of the total grains based on the morphotype classification (Fig. 9).

In the Eastern Unit, the lengths were 44–142 (B0, mean: 86.2 μm), 49–131 (B1, mean: 85.9 μm), 41–156 (B9, mean: 83.7 μm), 38–142 (C1, mean: 83.7 μm), 42–133 (C2, mean: 82.8 μm), and 43–154 μm (C3, mean: 89.6 μm) and their widths were 34–121 (B0, mean: 57.7 μm), 34–95 (B1, mean: 62.0 μm), and 35–144 (B9, mean: 56.1 μm), 34–128 (C1, mean: 61.8 μm), 34–90 (C2, mean: 56.9 μm), and 35–116 μm (C3, mean: 64.6 μm) (Fig. 8 and Table 2). The mean elongation values (width/length) were 0.69 (B0, B9), 0.73 (B1, C3), 0.72 (C1), and 0.70 (C2) (Fig. 8 and Table 2), and mean roundness values were 4.4 (B0, B9, C1, C2, C3) and 3.9 (B1) (Fig. 8 and Table 2), and they were generally euhedral, angular or slightly rounded. Based on the morphotype classification (Pupin, 1980), S19 and S24 types accounted for more than 10%, and S7, S12, S13, S18, S23, and G1–3 types occupied more than 5% of the total grains (Fig. 9).

5.2.2. Back-arc deposits (Maizuru Belt)

Ohkawa et al. (2022) examined the detrital zircon ages and morphology of four sandstone samples from the middle Permian sedimentary succession, Maizuru Belt. They measured total spots of 247 and 239 and obtained concordant ages of 214 and 212 from the sandstones of the lower and upper sedimentary succession, respectively. Furthermore, the morphotypes of 254 grains were classified (Fig. 9).

The shape and morphology of detrital zircons of the lower and upper successions showed different features (Fig. 8 and Table 2). In the lower succession, the lengths from samples 190803-04 and 190803-03 were 54–211 (mean: 106.3 μm) and 40–217 μm (mean: 104.1 μm), and their widths were 33–137 μm (mean: 59.3 μm) and 35–98 μm (mean: 59.9 μm), respectively (Fig. 8 and Table 2). The mean elongation values (width/length) of samples 190803-04 and 190803-03 were 0.58 and 0.61, respectively. The mean roundness values were 3.1 (190803-04) and 3.4 (190803-03) (Fig. 8 and Table 2), and they were generally euhedral,

angular, or slightly rounded. On the other hand, the lengths from the upper succession (samples 180502-05 and 190803-01) were 48–151 (mean: 92.8 μm) and 57–171 μm (mean: 110.4 μm), and their widths were 41–109 (180502-05, mean: 62.1 μm) and 37–122 μm (190803-01, mean: 74.5 μm), respectively (Fig. 8 and Table 2). The mean elongation values from samples 180502-05 and 190803-01 were 0.69, and the mean roundness values were 6.1 and 6.3, respectively (Fig. 8 and Table 2). The grains were generally well-rounded, and the crystal faces were few recognizable. In the morphotype classification of the lower succession, S24 and S25 types accounted for more than 15%, and S19, S23, and G1–3 types occupied more than 10% of the total grains (Fig. 9). In the upper succession, S24 type accounted for more than 15%, and S18, S25, and G1–3 types occupied more than 10% of the total grains (Fig. 9).

5.3. U–Pb ages of the detrital zircons

The age spectra of the detrital zircons are shown in Fig. 10, and the relationships among age and shape, morphotype, and Th/U ratio are shown in Figs. 11 and 12.

5.3.1. Fore-arc deposits (Akiyoshi Belt)

In the Western Unit, the age spectra of the detrital zircons indicated a unimodal distribution. They were dominated by Permian age (>90%), whereas pre-Permian age components rarely contained (Fig. 10). The ages from samples A2 and A9 were 247.5–1866.0 and 243.8–565.0 Ma, respectively (Fig. 10). The grains of 77 (A2) and 82% (A9) indicated high Th/U ratios (≥0.5) typical of an igneous source (Hoskin and Schaltegger, 2003; Kirkland et al., 2015). On the other hand, one grain of A9 show low Th/U ratios (≤0.1) characteristic of a metamorphic source (Rubatto and Hermann, 2003; Rubatto, 2017) (Fig. 12).

In the Eastern Unit, the age spectra of the detrital zircons showed a single peak the same as those of the Western Unit, and the majority (i.e., more than 70%) of these grains are Permian age. The sandstones of Route B (B0, B1, B9) contained Carboniferous age components of ca. 8–16% and Precambrian age components of ca. 5–9%. The sandstones of Route C (C1, C2, C3) contained Carboniferous age components of ca. 5–8% (Fig. 10). The ages were 250.8–3374.0 (B0), 253.5–1947.0 (B1), 248.5–2570.0 (B9), 246.5–864.0 (C1), 251.8–324.5 (C2), and 249.9–479.5 Ma (C3) (Fig. 10). The grains of 69 (B0), 73 (B1), 84 (B9), 77 (C1), and 79% (C2 and C3) indicated high Th/U ratios (≥0.5) characteristic of an igneous origin (Hoskin and Schaltegger, 2003; Kirkland et al., 2015). On the other hand, one (B0 and C3) and two grains (B9) show low Th/U ratios (≤0.1) typical of a metamorphic origin (Rubatto and Hermann, 2003; Rubatto, 2017) (Fig. 12).

5.3.2. Back-arc deposits (Maizuru Belt)

The age spectra of detrital zircons of the lower and upper successions showed different characteristics by Ohkawa et al. (2022). The age spectra of the lower succession showed a single peak, and they were dominated by Permian age (>90%). The ages from samples 190803-04 and 190803-03 were 262.0–319.0 and 258.2–302.4 Ma, respectively (Fig. 10). Most grains of 81 (190803-04) and 94% (190803-04) indicated high Th/U ratios (≥0.5) typical of an igneous source (Hoskin and Schaltegger, 2003; Kirkland et al., 2015). On the other hand, the sandstones did not contain low Th/U (≤0.1) zircon typical of a metamorphic origin (Rubatto and Hermann, 2003; Rubatto, 2017) (Fig. 10).

The age spectra of the upper succession contained spread age components of 2500–1800 and 500–270 Ma. They contain Precambrian ages of 29–42%, whereas the ratio of Permian age is low (8–17%). The ages from samples 180502-05 and 190803-01 were 2730–269.5 and 2666–269.8 Ma, respectively (Fig. 10). The grains of 54 (180502-05) and 60% (190803-01) had high Th/U ratios (≥0.5) characteristic of an igneous origin. One (190803-01) and three (180502-05) grains indicated low Th/U ratios (≤0.1) typical of a metamorphic origin (Fig. 12).

6. Discussion

6.1. Depositional environments based on crystal morphologies and U–Pb ages of detrital zircons

This study discussed the depositional environments and provenance of fore- and back-arc deposits based on the relationship between crystal morphologies and U–Pb ages of detrital zircons (Figs. 10–14). For discussing a change of depositional evolution of the entire Akiyoshi and Maizuru Belts, we compared published detrital zircon age data from Akiyoshi (middle to late Permian sedimentary succession of Nishiki area, Yamaguchi Prefecture) and Maizuru Belts (middle Permian sedimentary succession of Tsuwano area, Shimane Prefecture) (Zhang et al., 2018a; Kimura et al., 2021) with measured data by this study and Ohkawa et al. (2022) (Figs. 13 and 14). The result indicates that the sandstones from fore- and back-arc deposits can be divided into two groups (Groups A and B) (Fig. 14). Sandstones of Group A mainly contained the late Paleozoic age components close to the depositional age, and the grains were generally angular to subangular. On the other hand, Sandstones of Group B yielded broad age components from Precambrian to Paleozoic, and the grains were commonly rounded.

In the fore- and back-arc deposits at convergent plate margins, the zircons show the features that they are angular and subangular and do not contribute from recycling and chemical

weathering, and their ages are close to the deposition age (Cawood et al., 2012; Gibson et al., 2013; Ohkawa et al., 2021, 2022). The cumulative proportion curves from Permian fore-arc deposits and a part of the Permian back-arc deposits (190803-03 and 190803-04) plotted in a convergent setting (Fig. 14). These zircons consisted mainly of late Paleozoic age components near to the depositional age, and they were angular to subangular and well-defined crystal faces (Zhang et al., 2018a; Ohkawa et al., 2022; this study) (Figs. 7, 8, 10, 11, and 13). Moreover, these age spectra belong to a close group (Group A) based on MDS analysis (Fig. 14). The detrital zircon was reported to become rapidly rounded under arid climate conditions (Garzanti et al., 2012, Garzanti et al., 2015). However, Gärtner et al. (2022) reported that the smallest zircon grains of dune sands are rarely shorter than 60 µm. It is suggested that the influence of the aeolian environment is small because the late Paleozoic zircons of Groups A and B were commonly less rounded and contained small grains (< 60 µm) (Figs. 8 and 11). On the other hand, there are some opinions on between the detrital zircon shape and transport distance (Zoleikhaei et al., 2016; Markwitz et al., 2017; Gärtner et al., 2018; Sundell et al., 2018; Zeh and Wilson, 2022). However, some researchers suggested that the zircon grains become rounded with increasing transport distance by shape analysis of detrital zircon (Markwitz et al., 2017; Sundell et al., 2018). Moreover, several studies reported that zircon shape is affected by hydrodynamic conditions during transport (Zeh and Cabral, 2021; Zeh and Wilson, 2022), and Zeh and Wilson (2022) reported that zircon grains from shallow-marine deposits were subjected to hydrodynamic sorting and abrasion related to marine transgression, and transport, sorting and abrasion of grains derived from wave action, tides, storm activity, and off-shore currents. The zircons of Group A derived mainly from igneous origin based on the Th/U ratios and structures (Zhang et al., 2018a; Ohkawa et al., 2022; this study). Furthermore, the Qm–F–Lt and Lm–Lv–Ls plots for the Permian sandstones of the Maizuru and Akiyoshi Belts support that most of them are igneous arc origin (Fig. 6). Therefore, the sandstones of Group A had similar sources, and they were located near the depositional sites. The provenance mainly had igneous rocks derived from the late Paleozoic volcanic arc, and the rocks were considered to be exposed immediately prior to their erosion and transport, and were transported directly to the depositional site in a relatively short time.

Based on the above results, the zircon shapes and age spectra of Group A show similar features. However, the roundness and elongation of Group A of the Akiyoshi Belt are slightly different from those of the Maizuru Belt, and the mean roundness and elongation of zircons in the Akiyoshi Belt are higher than those of the Maizuru Belt (Fig. 8 and Table 2). Kimura (1988) reported that the sandstones of the Maizuru Belt contain the rock fragments (especially mafic

and sedimentary rock fragments) than those of the Ultra-Tamba Belt (Permian fore-arc accretionary complex) based on a comparison of sandstone compositions. Kimura (1988) suggested that the source of the Ultra-Tamba Belt was farther than that of the Maizuru Belt, and unstable rock fragments were destroyed in the transport process. The rock fragments of the sandstones of the Akiyoshi Belt tend to be small amount than those of the Maizuru Belt (Fig. 6). Furthermore, the mudstones of the Permian sedimentary succession of the Maizuru Belt were considered to be deposited in a quiet shallow sea based on lithology and geochemical features (Shimizu, 1962b; Mavoungou et al., 2022). Based on the above results, the zircon shape of samples 190803-03 and 190803-04 from the mudstone-dominated succession in the Maizuru Belt indicates that they were supplied from near sources and weak hydrodynamic conditions, supporting the depositional environments of the mudstone inferred from previous studies. On the other hand, clastic rocks in the Akiyoshi Belt in the Itoigawa and Nishiki areas were estimated to be deposited in the trench and trench-slope basin, suggesting that the detritus was supplied by sediment gravity flow such as debris flow and turbidity current (Tanaka et al., 1987; Hara and Kiminami, 1989; Matsuzawa and Takeuchi, 2009). Based on the difference in depositional environments between the Akiyoshi and Maizuru Belts, the slightly higher roundness and elongation of the detrital zircons in the Akiyoshi Belt support that they may be subjected to strong hydrodynamic conditions in the marine environment and long-distance transport from the volcanic arc to the trench.

On the other hand, some sandstones in the Maizuru Belt (samples 180502-05, 190803-01, and TWN-SS01) commonly contained zircon grains that were older than their depositional ages (Kimura et al., 2022; Ohkawa et al., 2022), and the cumulative proportion curve of sample 190803-01 belong to collisional setting (Fig. 14). In sediments of the collisional and extensional settings, the detrital zircons were generally rounded and much older than their depositional ages, suggesting that they derived mainly from long-distance transport (Cawood et al., 2012; Kydonakis et al., 2014; Xu et al., 2019; Ohkawa et al., 2022). Ohkawa et al. (2022) reported that zircon grains of samples 180502-05 and 190803-01 had unclear crystal faces and well-rounded edges the same as those of deposits supplied from collisional zones (Figs. 7, 8, 10, 11, and 13). Based on MDS analysis, these age spectra belonged to a close group (Group B) and were distributed apart from those of Group A (Fig. 14). Therefore, the sandstones of Group B had similar sources containing older continental crust, suggesting that they had distant sources that were first cycle or recycled, and/or strong hydrodynamic conditions during transport. Moreover, changes of the zircon ages and morphology from the middle Permian sedimentary succession in the Maizuru Belt support that the provenance changed from a

convergent setting to a collisional setting during the middle Permian (Ohkawa et al., 2022).

Mavoungou et al. (2022) suggested that breccia (Tonoshiki breccia) of the Permian sedimentary succession in the Maizuru Belt was debris sediments with submarine slope failures and intense tectonic activity with collision occurred during the deposition by petrological and geochemical characteristics. The upper succession of the Maizuru Belt in the Itoigawa area consisted mainly of breccia, and it had mostly angular shapes and contained fragments of various sizes and types, such as mafic and felsic igneous and sedimentary rock (Nagamori et al., 2010), the same as those of the Tonoshiki breccia. Therefore, the breccia was suggested to be supplied by the debris flow characterized by submarine slope failures and short-transport distance. The above results support that the zircons of Group B were affected by strong hydrodynamics in the marine environment during transport. Moreover, the breccia and sandstone of the Maizuru Belt contained sedimentary and meta-sedimentary rock fragments (e.g., Suzuki et al., 1982; Nagamori et al., 2010; Mavoungou et al., 2022; Ohkawa et al., 2022). Therefore, some rounded zircons may be affected by long-distance transport resulting from multiple sedimentary cycles. The Qm–F–Lt plot shows that the Permian sandstones of the Maizuru Belt were mainly plotted in magmatic arc fields, whereas the Triassic sandstones were plotted in the magmatic arc, recycled orogen, and mixed fields (Fig. 6). Therefore, the change of sandstone compositions in the Maizuru Belt indicates that the provenance changed from volcanic arc to multiple sources containing older continental block. This result is consistent with previous studies that the Maizuru Belt was an island arc–back-arc basin–continental crust system and collided during the Permian (Mavoungou et al., 2022; Ohkawa et al., 2022).

6.2. Provenance of the fore-arc and back-arc deposits

As described in Section 2, igneous rocks are distributed in the Southern and Northern Maizuru Belt (e.g., Hayasaka, 1996), suggesting that some clastic rocks in the Maizuru and Akiyoshi Belts were supplied from those igneous rocks (Kano, 1961; Kano et al., 1961; Takeuchi et al., 2008). The Permian sandstones of the Akiyoshi and Maizuru Belts are suggested to be derived mostly from igneous sources based on their sandstone compositions and zircon Th/U ratio and structure. Based on U–Pb ages of the granitoid, island arc magmatism occurred at 285–275 Ma (Herzig et al., 1997). These ages are consistent with the major age component of Group A (Figs. 10 and 13). As discussed in Section 6.1, sandstones of Group A suggest they deposited around a volcanic arc formed by late Paleozoic igneous activity. Because the lithological and geochemical features of the granitoids of the Southern Maizuru Belt indicated that they formed in an intra-oceanic island arc (Suda and Hayasaka, 2009), the

sandstones of the Group A are considered to be supplied mainly from an island arc (containing igneous rocks of the Southern Maizuru Belt) isolated from the older continental crust.

On the other hand, the detrital zircons of Group B contained wide age groups of Precambrian to Paleozoic, and their age distribution differed from those of the igneous rocks of the Southern Maizuru Belt (Figs. 10 and 13). Furthermore, it is inferred that sediments of the Maizuru Belt were supplied from multiple sources, such as the volcanic arc and Precambrian continental block (Fig. 6). The igneous rocks of the Northern Maizuru Belt are suggested to be intruded during the Silurian to Devonian and Permian to Triassic based on the U–Pb zircon ages (Fujii et al., 2008; Tsutsumi et al., 2014). Kimura et al. (2019, 2021) reported an Archean–Paleoproterozoic continental unit from the westernmost part of the Maizuru Belt, which consisted of ca. 2700–2500 Ma granitic gneiss (containing zircon rims of low Th/U ratio), ca. 2430 Ma metaquartzite (ca. 1850 Ma metamorphism), ca. 1900–1825 Ma granitoid, and ca. 440–410 Ma granitoid, felsic tuff, and metagabbro. They suggested that this unit was contrasted with the rocks of the Northern Maizuru Belt and the Sino–Korean Block by lithology and isotopic ages. The ages of the igneous and metamorphic rocks of the Northern Maizuru Belt are consistent with the age components of Group B (Kimura et al., 2021; Ohkawa et al., 2022). These results support that the sandstones of Group B were supplied from the rocks of the Northern Maizuru Belt and its associated neighboring continental crust (Sino-Korean Block) (Kimura et al., 2021; Ohkawa et al., 2022). A part of pre-late Paleozoic detrital zircons in the Maizuru and Akiyoshi Belts indicated features of a metamorphic origin, such as the low Th/U ratio (Rubatto and Hermann, 2003; Rubatto, 2017) and homogeneous structure (Corfu et al., 2003) (Fig. 7). They are considered to be supplied from Precambrian to Paleozoic metamorphic and metasedimentary rocks in the Northern Maizuru Belt (Ohkawa et al., 2022).

Many researchers have reported that the zircon morphotype provided information about the host rock (e.g., Pupin, 1980; Tietz et al., 2003; Belousova et al., 2006; Gärtner et al., 2017; Zieger et al., 2019; Ohkawa et al., 2022). The morphotype classification of zircon by Pupin (1980) can interpolate information on the chemical and thermal characteristics of the crystallization medium. The Permian sandstones of the Akiyoshi and Maizuru Belts commonly contain the main morphotypes of G1–3 and S24 (Fig. 9). Type G1–3 zircons show well-developed {110} prism and {101} pyramid, and type S24 zircons show a predominance of {100} prism and the presence of two pyramids; one well-developed {101} and other weakly developed {211}. Furthermore, the major morphotypes of the Akiyoshi and Maizuru Belts contain S7, S19 and S18, S25, respectively (Fig. 9). Type G1–3 derived from relatively low-temperature (550–650°C) and calc-alkaline granites of hybrid (crustal and mantle) origin or I-

type granites of mantle or mainly mantle origin (Pupin, 1980; Belousova et al., 2006). Types S18, S19, S24, and S25 are suggested to be derived from relatively high-temperature (750–900°C) and calc-alkaline granites of hybrid (crustal and mantle) origin or magmatic charnockite or I-type granites of mantle or mainly mantle origin (Pupin, 1980; Belousova et al., 2006). Type S7 originated from migmatite or S-type granites of crustal or mainly crustal origin (Pupin, 1980; Belousova et al., 2006). The zircon morphotype of the igneous rocks in the Maizuru Belt has never been reported before. However, Paleozoic granitoids in Japan containing the Maizuru Belt mainly belong to the calc-alkaline series (Kobayashi et al., 2000; Suda and Hayasaka, 2009 and references therein) and I-type granites (Kobayashi et al., 2000) based on geochemical characteristics. Moreover, migmatites were recognized in the Southern Maizuru Belt (Suda and Hayasaka, 2009). Therefore, the morphological characteristics of the zircons of Groups A and B support that they originated mainly from the rocks of the Southern and Northern Maizuru Belt.

6.3. Tectonic evolution of Permian fore-arc and back-arc tectonic evolution of the proto-Japan and East Asia

In this section, we discuss the tectonic evolution of East Asia and proto-Japan, by combining comprehensive data of sandstone compositions and detrital zircon ages and morphology from the Permian fore- (Akiyoshi Belt) and back-arc (Maizuru Belt) deposits with regional geological information, and constrain the timing of collisional movement (Fig. 15).

As discussed in Section 6.2, the Permian fore-arc deposits were deposited around the volcanic arc isolated from the Sino–Korean Block (Fig. 15). The sandstones of the Akiyoshi Belt mainly contain late Paleozoic zircon grains that derived from the volcanic arc, but it should not be missed that they slightly contain Precambrian to middle Paleozoic grains (Figs. 10, 11, and 13). These ages are also found in those of the Maizuru Belt (Figs. 10, 11, and 13). Moreover, sample B0 of the Akiyoshi Belt, which contains Precambrian age of 5 %, and sample TWN-SS01 of the Maizuru Belt have similarities based on the MDS analysis (Fig. 14). Although information about the transportation route of their detritus has never reported before, most of the grains are well-rounded, and the crystal faces are hardly recognizable (Fig. 11). Based on the zircon age and shape, these grains derived from the rocks of the Sino–Korean Block and were affected by long-distance transportation. Tsutsumi et al. (2000) also suggested that the provenance of the Akiyoshi Belt was partly the rocks of the Sino–Korean Block by U–Pb dating of acidic tuff. Furthermore, late Permian to Early Triassic ages were reported from the sandstones in the Akiyoshi Belt and igneous rocks of the Northern Maizuru Belt in common

18

(Fujii et al., 2008; Tsutsumi et al., 2014). Because igneous rocks of the Southern Maizuru Belt indicated early Permian age (Herzig et al., 1997) and were slightly older than those of the sandstones, the late Paleozoic to early Mesozoic zircons in the Akiyoshi Belt are considered to be partly supplied by igneous rocks in the Northern Maizuru Belt (Fig. 15b and c). The similarity of the detrital zircon age spectra of the Maizuru and Akiyoshi Belts supports previous studies that both belts had a close relationship (e.g., Takeuchi et al., 2008; Tazawa et al., 2009). Sandstone compositions of the Akiyoshi Belt were considered to increase the ratio of plutonic to volcanic sources in ascending stratigraphic order by uplift and denudation of the volcanic arc (Zhang et al., 2018) (Fig. 6). This change has been reported from Permian to Triassic fore-arc deposits in Southwest and Northeast Japan (e.g., Yoshida and Tazawa, 2000; Yoshida and Machiyama, 2004; Ohkawa et al., 2021). Until now, the cause of Permian to Triassic tectonic movement with uplift and denudation of the volcanic arc has been unknown. However, a comparison of sandstone compositions, detrital zircon ages, and morphology from the Akiyoshi and the Maizuru Belts, which were deposited at the same latitude, suggests that the sandstone compositions in the Akiyoshi Belt changed during or after the proto-Japan's collision (Ohkawa et al., 2022) (Fig. 6). Therefore, there is a high possibility that provenance change with progressive denudation of the volcanic arc derived from the collision and suture of the proto-Japan with East Asian's continental block.

The variation of zircon age spectra and morphology of the Maizuru Belt represents the depositional environment and tectonic evolution of the back-arc basin accompanied by the collision between the proto-Japan and Sino–Korean Block. The Maizuru Belt was suggested to form a back-arc basin (Maizuru back-arc basin) during the early Permian because of the occurrence of early Permian back-arc basin basalts (Suda et al., 2014; Mavoungou et al., 2022). In the middle Permian, the back-arc basin was a quiet shallow sea, and the mudstone-dominated sequence was deposited (Shimizu, 1962b; Mavoungou et al., 2022) (Fig. 15). The detrital zircon ages and morphology of the Group A in the Maizuru Belt suggest that they deposited at the weak hydrodynamic conditions, and were supplied directly from nearby sources (Fig. 8 and Table 2). Then, debris flow deposits consisted mainly of the breccia were deposited during the closure of the Maizuru back-arc basin at the late Permian to the Triassic (Mavoungou et al., 2022) (Fig. 15). The detrital zircons of the Group B in the Maizuru Belt suggest that they were supplied from distance sources and deposited at the strong hydrodynamic conditions such as debris flow, and they derived from the Northern and Southern Maizuru Belts (Ohkawa et al., 2022) (Fig. 8 and Table 2). Mavoungou et al. (2022) inferred that the breccia partly derived from the Permian sedimentary succession of the Maizuru Belt and was supplied by submarine

slope failures based on petrological and geochemical characteristics of the breccia. Group B of the Maizuru Belt contains late Paleozoic well-rounded zircon grains (Fig. 11). These grains are considered to have experienced significant abrasion caused by multiple transportations with recycling, slope failure, and debris flow. Furthermore, some Precambrian grains may have experienced long transportation from the continental crust to the back-arc basins. The changes of the depositional environment, detrital zircon ages, and morphology of the back-arc basin deposits suggest that the provenance changed from the convergent to the collisional settings during the middle Permian (Ohkawa et al., 2022). This result supports previous studies that collisional orogeny occurred in proto-Japan and East Asia during the late Paleozoic and early Mesozoic (e.g., Faure and Charvet, 1987; de Jong et al., 2009; Suda et al., 2014; Mavoungou et al., 2022; Ohkawa et al., 2022). As mentioned above, the supply of detrital grains derived from older continental crust began in the back-arc basin during the Permian, whereas Permian sandstones in the fore-arc deposits rarely contained Precambrian zircon grains. It is suggested that the sediments derived from older continental crust were trapped in a back-arc basin and blocked by topographic barriers of the uplift zone of the volcanic arc (Ohkawa et al., 2021). However, a small amount of detritus originating from the continental crust was supplied to the fore-arc.

The ages of some Paleozoic igneous rocks, the stratigraphy of shelf deposits, and the detrital zircon age spectra of Permian sandstones in Japan are correlated with the eastern CAOB containing the Khanka Block (e.g., Fujii et al., 2008; Suzuki and Kurihara, 2021; Ohkawa et al., 2022). On the other hand, εHf(t) values of detrital zircons from the Akiyoshi Belt were suggested to correlate with the South China Block (Zhang et al., 2019). Permian brachiopod faunas of the proto-Japan varied depending on the region and were widely correlated with South China and Sino–Korean Blocks and South Primorye (Far East Russia) (e.g., Tazawa, 2001). Permian volcanic activity was reported from Hainan Island (Li et al., 2006; Shen et al., 2018), the southeastern part of the Korean Peninsula (e.g., Yi et al., 2012; Choi et al., 2021; Kim et al., 2021), and Jiamusi-Khanka-Bureya block (e.g., Yang et al., 2015, 2017, Bi et al., 2017; Zhang et al., 2018b). Eisenhauer and Zhao (2018) proposed the region east of the Songliao, Erguna, and Xing'an blocks characterized by ca. 500 Ma high-grade metamorphosed rocks for the Jiamusi-Khanka-Bureya block. These activities are considered to be arc-type magmatism associated with the westward subduction of the Paleo-Pacific plate (e.g., Shen et al., 2018; Yang et al., 2015, 2017), and they have continued to the Triassic (e.g., Li et al., 2006; Yang et al., 2015, 2017; Shen et al., 2018; Choi et al., 2021; Kim et al., 2021), the same as those of the Maizuru Belt. Based on these results, it is suggested that the Permian volcanic arc

with proto-Japan has formed along the subduction of the Paleo-Pacific Plate in the eastern margin of East Asia (de Jong et al., 2009; Ohkawa et al., 2021), and the subduction may have continued from the Jiamusi-Khanka-Bureya block through proto-Japan to South China Block. de Jong et al. (2006) considered that the extension of the Solonker Suture Zone, which is marked by the tectonic boundary between the Sino–Korean Block and CAOB, extends from the Jilin area to the Korean Peninsula based on regional geological information of East Asia. A part of pre-late Paleozoic zircon grains such as ca. 500 Ma zircons of the Permian sandstones of the Maizuru Belt was suggested to be supplied by the CAOB (Kimura et al., 2021; Ohkawa et al., 2022). These results support that the extension of the Solonker Suture Zone continued to the Maizuru back-arc basin (Fig. 15). This study supports previous models in which the proto-Japan was distributed near to the Sino–Korean Block and eastern CAOB during the Permian (de Jong et al., 2009; Ohkawa et al., 2022) (Fig. 15), and does not support the models that the proto-Japan was distributed around the South China Block (Hara et al., 2018; Zhang et al., 2018a, 2019) or was oceanic island arc isolated from the older continental block (Nakama et al., 2010; Okawa et al., 2013; Suzuki and Kurihara, 2021). The proto-Japan began to collide and suture with the Sino–Korean Block during the middle Permian, and a large amount of detritus was supplied to the fore- and back-arc (Fig. 15). Sandstone compositions and detrital zircon data of fore- and back-arc deposits of the proto-Japan constrain changes of orogenic movements and depositional environments associated with the collision, and may provide the key to discussing the spatial distribution of volcanic activity and the subduction of the Paleo-Pacific plate margin. However, the tectonics and evolution of East Asia should be carefully discussed because the eastern margin of East Asia containing proto-Japan has undergone re-arrangement by strike-slip movements and other tectonic events at the post-Paleozoic (e.g., Faure and Natal'in, 1992; Isozaki et al., 2010).

7. Conclusion

Published and new measured data of detrital zircon age and morphology from Permian fore- and back-arc deposits in Japan provided the following information:

1. The fore- and a part of back-arc deposits mainly contain the late Paleozoic zircon grains that are close to their depositional ages and commonly less rounded. These grains were derived mainly from a late Paleozoic volcanic arc and were transported directly to the depositional site in a relatively short time.

2. A part of back-arc deposits generally contains Precambrian to Paleozoic zircon grains that are commonly older than their depositional ages and well-rounded. These grains

were derived from multiple sources (the volcanic arc and Sino-Korean Block), and were affected by long-distance transportation and strong hydrodynamics during transport.

3. Comprehensive detrital zircon data in the fore- and back-arc deposits support that the island arc–back-arc basin–continental margin system has been formed along the eastern margin of East Asia, and the volcanic arc collided with the eastern margin of Sino–Korean Block during the Permian.

Reference

Andersen, T., Kristoffersen, M., Elburg, M. A., 2018. Visualizing, interpreting and comparing detrital zircon age and Hf isotope data in basin analysis−a graphical approach. Basin Research, 30, 132-147.

Bailey, E. H., Stevens, R. E., 1960. Selective staining of K-feldspar and plagioclase on rock slabs and thin sections. American Mineralogist: Journal of Earth and Planetary Materials, 45, 1020-1025.

Belousova, E. A., Griffin, W. L., O'Reilly, S. Y., 2006. Zircon crystal morphology, trace element signatures and Hf isotope composition as a tool for petrogenetic modelling: examples from Eastern Australian granitoids. Journal of Petrology, 47, 329-353.

Bi, J. H., Ge, W. C., Yang, H., Wang, Z. H., Dong, Y., Liu, X. W., Ji, Z., 2017. Age, petrogenesis, and tectonic setting of the Permian bimodal volcanic rocks in the eastern Jiamusi Massif, NE China. Journal of Asian Earth Sciences, 134, 160-175.

Cawood, P. A., Hawkesworth, C. J., Dhuime, B., 2012. Detrital zircon record and tectonic setting. Geology. 40, 875−878.

Choi, H. O., Choi, S. H., Kim, S. S., 2021. Zircon U-Pb geochronology and Sr–Nd–Pb–Hf isotope geochemistry for Permian–Early Triassic arc-related magmatism in Pohang, Jangsari, and Yeongdeok, southeastern Korean Peninsula. Lithos, 382, 105930.

Corfu, F., Hanchar, J. M., Hoskin, P. W., Kinny, P., 2003. Atlas of zircon textures. Reviews in mineralogy and geochemistry, 53, 469-500.

de Jong, K., Xiao, W., Windley, B. F., Masago, H., Lo, C. H., 2006. Ordovician 40Ar/39Ar

phengite ages from the blueschist-facies Ondor Sum subduction-accretion complex (Inner Mongolia) and implications for the early Paleozoic history of continental blocks in China and adjacent areas. American journal of Science, 306, 799-845.

de Jong, K., Kurimoto, C., Ruffet, G., 2009. Triassic ^{40}Ar/^{39}Ar ages from the Sakaigawa unit, Kii Peninsula, Japan: implications for possible merger of the Central Asian Orogenic Belt with large-scale tectonic systems of the East Asian margin. International Journal of Earth Sciences. 98, 1529−1556.

Dickinson, W. R., 1970. Interpreting detrital modes of graywacke and arkose. Journal of Sedimentary Research, 40, 695-707.

Dickinson, W.R., 1985. Interpreting provenance relations from detrital modes of sandstones. In: Zuffa, G.G. (Ed.), Provenance of Arenites. Reidel, Dordrecht, NATO ASI Series 148, pp. 333–361.

Dickinson, W. R., Gehrels, G. E., 2009. Use of U–Pb ages of detrital zircons to infer maximum depositional ages of strata: a test against a Colorado Plateau Mesozoic database. Earth and Planetary Science Letters, 288, 115-125.

Ehiro, M., 2000. Relationships in tectonic framework among the South Kitakami and Hayachine Tectonic Belts, Kurosegawa Belt, and "Paleo-Ryoke Belt". Mem. Geol. Soc. Japan. 56, 53–64 (in Japanese with English abstract).

Ehiro, M., 2001. Origins and drift histories of some microcontinents distributed in the eastern margin of Asian Continent (< Special issue> Geotectonic framework of eastern Asia before the opening of the Japan Sea). Earth Science (Chikyu Kagaku). 55, 71–81.

Ehiro, M., 2017, Chapter 4.2. South Kitakami Belt. In Geological Society of Japan, ed., Regional Geology of Japan, Vol. 2, Tohoku Region, edited by Yoshida, T., Asakura Publ., pp.184–240.

Eizenhöfer, P. R., Zhao, G., 2018. Solonker Suture in East Asia and its bearing on the final closure of the eastern segment of the Palaeo-Asian Ocean. Earth-Science Reviews, 186, 153-172.

Faure, M., & Natal'in, B., 1992. The geodynamic evolution of the eastern Eurasian margin in Mesozoic times. Tectonophysics, 208, 397-411.

Faure, M., Charvet, J., 1983. Tangential tectonics in the Chichibu zone from the example of E. Shikoku. Proceedings of the Japan Academy, Series B, 59, 117−120.

Faure, M., Charvet, J., 1987. Late Permian/early Triassic orogeny in Japan: piling up of nappes, transverse lineation and continental subduction of the Honshu block. Earth and Planetary Science Letters, 84, 295−308.

Fildani, A., Cope, T. D., Graham, S. A., Wooden, J. L., 2003. Initiation of the Magallanes foreland basin: Timing of the southernmost Patagonian Andes orogeny revised by detrital zircon provenance analysis. Geology, 31, 1081-1084.

Folk, R. L., 1968. Petrology of sedimentary rocks. Hemphill publishing company, USA, 170 pp.

Folk, R. L., 1980. Petrology of sedimentary rocks. Hemphill publishing company, USA, 182 pp.

Fujii, M., Hayasaka, Y., Terada, K., 2008. SHRIMP zircon and EPMA monazite dating of granitic rocks from the Maizuru terrane, southwest Japan: Correlation with East Asian Paleozoic terranes and geological implications. Island Arc. 17, 322−341.

Garzanti, E., Andò, S., Vezzoli, G., Lustrino, M., Boni, M., Vermeesch, P., 2012. Petrology of the Namib Sand Sea: Long-distance transport and compositional variability in the wind-displaced Orange Delta. Earth-Science Reviews, 112, 173-189.

Garzanti, E., Resentini, A., Andò, S., Vezzoli, G., Pereira, A., Vermeesch, P., 2015. Physical controls on sand composition and relative durability of detrital minerals during ultra-long distance littoral and aeolian transport (N amibia and southern A ngola). Sedimentology, 62, 971-996.

Gehrels, G., 2014. Detrital zircon U−Pb geochronology applied to tectonics. Annual Review of Earth and Planetary Sciences. 42, 127−149.

Gehrels, G.E., Valencia, V.A., Ruiz, J., 2008. Enhanced precision, accuracy, efficiency, and spatial resolution of U−Pb ages by laser ablation−multicollector−inductively coupled plasma−mass spectrometry. Geochemistry, Geophysics, Geosystems. 9.

Gibson, T. M., Myrow, P. M., Macdonald, F. A., Minjin, C., Gehrels, G. E., 2013. Depositional history, tectonics, and detrital zircon geochronology of Ordovician and Devonian strata in southwestern Mongolia. Bulletin, 125, 877-893.

Gärtner, A., Linnemann, U., Sagawe, A., Hofmann, M., Ullrich, B., Kleber, A., 2013. Morphology of zircon crystal grains in sediments−characteristics, classifications, definitions. Geol. Saxonica 59, 65−73.

Gärtner, A., Youbi, N., Villeneuve, M., Linnemann, U., Sagawe, A., Hofmann, M., Zieger, J., Mahmoudi, A., Boumehdi, M. A., 2018. Provenance of detrital zircon from siliciclastic rocks of the Sebkha Gezmayet unit of the Adrar Souttouf Massif (Moroccan Sahara)−Palaeogeographic implications. Comptes Rendus Geoscience, 350, 255-266.

Gärtner, A., Youbi, N., Villeneuve, M., Sagawe, A., Hofmann, M., Mahmoudi, A., Boumehdi, M. A., Linnemann, U., 2017. The zircon evidence of temporally changing sediment

transport—the NW Gondwana margin during Cambrian to Devonian time (Aoucert and Smara areas, Moroccan Sahara). International Journal of Earth Sciences, 106, 2747-2769.

Gärtner, A., Hofmann, M., Zieger, J., Sagawe, A., Krause, R., Stutzriemer, M., Gesang, S., Gerdes, A., Marko, L., Lana, C., Linnemann, U., 2022. Implications for sedimentary transport processes in southwestern Africa: a combined zircon morphology and age study including extensive geochronology databases. International Journal of Earth Sciences, 111, 767-788.

Hada, S., Ishii, K. I., Landis, C. A., Aitchison, J., Yoshikura, S., 2001. Kurosegawa Terrane in Southwest Japan: Disrupted remnants of a Gondwana-derived terrane. Gondwana Research, 4, 27-38.

Hara, A. and Kiminami, K., 1989, Ancient Trench-fill and trench-slope basin deposits : an example from the Permian Nishiki Group, Southwest Japan. In Taira, A. and Masuda, F., eds., Sedimentary Facies in the Active Plate Margin, Terra Sci. Publ. Com., Tokyo, 557-575.

Hara, H., Hirano, M., Kurihara, T., Takahashi, T., Ueda, H., 2018. Permian arc evolution associated with Panthalassa subduction along the eastern margin of the South China block, based on sandstone provenance and U−Pb detrital zircon ages of the Kurosegawa belt, Southwest Japan. Journal of Asian Earth Sciences, 151, 112-130.

Hara, H., Ueki, T., Tsujino, Y., 2014. Geology of the Kitagawa District. Quadrangle Series, 1:50,000, Geological Survey of Japan. AIST, Japan, 72 pp (in Japanese with English abstract 4 p.).

Hayasaka, Y., 1996. Geological reconstruction of the Maizuru Terrane as an arc-back arc system. Tectonics and Metamorphism, 134-144 (in Japanese with English Abstract).

Herzig, C. T., Kimbrough, D. L., Hayasaka, Y., 1997. Early Permian zircon uranium-lead ages for plagiogranites in the Yakuno ophiolite, Asago district, Southwest Japan. Island Arc, 6, 396-403.

Hidaka, H., Shimizu, H., Adachi, M., 2002. U−Pb geochronology and REE geochemistry of zircons from Palaeoproterozoic paragneiss clasts in the Mesozoic Kamiaso conglomerate, central Japan: evidence for an Archean provenance. Chemical Geology. 187, 279−293.

Hoskin, P. W., Schaltegger, U., 2003. The composition of zircon and igneous and metamorphic petrogenesis. Reviews in mineralogy and geochemistry, 53, 27-62.

Ichikawa, K., 1990. Pre-Cretaceous terranes of Japan. International Geological Correlation Programme (IGCP), Japan, Pre-Cretaceous terranes of Japan pp. 1–12.

Ichiyama, Y., Ishiwatari, A., 2004. Petrochemical evidence for off-ridge magmatism in a back-

arc setting from the Yakuno ophiolite, Japan. Island Arc, 13, 157-177.

Igi, S., Kuroda, K., Hattori, H., 1961. Explanatory text of the geological map of Japan 1: 50,000: Maizuru. Kyoto, No.2. Geological Survey of Japan. AIST, Japan (in Japanese with English abstract).

Igi, S., Kuroda., 1965. Explanatory text of the geological map of Japan, Scale 1: 50,000: Oeyama. Kyoto, No.1. Geological Survey of Japan. AIST, Japan (in Japanese with English abstract).

Ingersoll, R. V., Suczek, C. A., 1979. Petrology and provenance of Neogene sand from Nicobar and Bengal fans, DSDP sites 211 and 218. Journal of Sedimentary Research, 49, 1217-1228.

Ingersoll, R. V., Bullard, T. F., Ford, R. L., Grimm, J. P., Pickle, J. D., Sares, S. W., 1984. The effect of grain size on detrital modes: a test of the Gazzi-Dickinson point-counting method. Journal of Sedimentary Research, 54, 103-116.

Ishiga, H., 1986. Late Carboniferous and Permian radiolarian biostratigraphy of Southwest Japan. Jour. Geosci. Osaka City Univ, 29, 89-100.

Ishiga, H., 1990. Paleozoic radiolarians. K Ichikawa, S Mizutani, I Hara, S Hada, A Yao (Eds.), Pre-Cretaceous terranes of Japan: Proc. Int. Geological Congr., Project No. 224, Pre-Jurassic Evolution of Eastern Asia, 285-290

Ishiwatari, A., Tsujimori, T., 2003. Paleozoic ophiolites and blueschists in Japan and Russian Primorye in the tectonic framework of East Asia: A synthesis. Island Arc, 12, 190-206.

Isozaki, Y., 1986. The Shingai Formation in the northern Chichibu Belt, Southwest Japan, and the end-Permian convergent zone along the northern margin of the Kurosegawa Landmass. Jour. Geol. Soc. Japan. 92, 497–516 (in Japanese with English abstract).

Isozaki, Y., Aoki, K., Nakama, T., Yanai, S., 2010. New insight into a subduction-related orogen: A reappraisal of the geotectonic framework and evolution of the Japanese Islands. Gondwana Research, 18, 82-105.

Isozaki, Y., Ehiro, M., Nakahata, H., Aoki, K., Sakata, S., Hirata, T., 2015. Cambrian plutonism in Northeast Japan and its significance for the earliest arc–trench system of proto-Japan: New U–Pb zircon ages of the oldest granitoids in the Kitakami and Ou Mountains. Journal of Asian Earth Sciences. 108, 136–149.

Kametaka, M., 1997. Provenance of the Upper Triassic Nariwa Group, Southwest Japan. Jour. Geol. Soc. Japan, 103, 880-896 (in Japanese with English abstract).

Kanmera, K., Nishi, H., 1983, Accreted oceanic reef complex in southwest Japan. In Hashimoto, M. and Uyeda, S., eds., Accretion tectonics in the circum-Pacific regions, Terra Publ. Co.,

Tokyo, pp.195-206.

Kano, H., 1961. On the'porphyroid'-like gneiss pebbles found in some conglomerates from the Maizuru district and their origin.-Petrographical contribution to the problem on the basement of the Japanese Islands (I). Journal of Geological Society of Japan, 67, 49-57 (in Japanese with English abstract).

Kano, H., Nakazawa, K., Igi, Y., Shiki, T., 1959. On the high-grade metamorphic rocks associated with the Yakuno intrusive rocks of the Maizuru zone. Journal of the Geological Society of Japan, 65, 267-271(in Japanese with English abstract).

Kano, H., Nakazawa, K., Shiki, T., 1961. Considerations on the Permian backgrounds of the Maizuru districts judging from the conglomerates. Jour. Geol. Soc. Japan, 67, 463-475 (in Japanese with English abstract).

Kawai M., Takeuchi M., 2001. Permian radiolarians from the Omi area in the Hida-gaien Tectonic Zone, central Japan News of Osaka Micropaleontologists, Spec., 12, pp. 23-32 (in Japanese with English abstract).

Kim, S. W., Kwon, S., Jeong, Y. J., Kee, W. S., Lee, B. C., Byun, U. H., Ko, K., Cho, D. L., Hong, P. S., Park, S. I., Santosh, M., 2021. The Middle Permian to Triassic tectono-magmatic system in the southern Korean Peninsula. Gondwana Research, 100, 302-322.

Kimura, K., 1988. Geology and tectonic setting of the Ultra-Tamba Belt in the western part of Ayabe City, Kyoto Prefecture, Southwest Japan. J. Geol. Soc. Japan. 94, 361−379 (in Japanese with English abstract).

Kimura, K., Hayasaka, Y., Shibata, T., Kawaguchi, K., Fujiwara, H., 2019. Discovery of Paleoproterozoic 1.85 Ga granitoid bodies from the Maizuru Terrane in the Tsuwano area, Shimane Prefecture, Southwest Japan and its geologic implications. Journal of the Geological Society of Japan, 125, 153-165 (in Japanese with English abstract).

Kimura, K., Hayasaka, Y., Yamashita, J., Shibata, T., Kawaguchi, K., Fujiwara, H., Das, K., 2021. Antiquity and tectonic lineage of Japanese Islands: New discovery of Archean−Paleoproterozoic Complex. Earth and Planetary Science Letters, 565, 116926.

Kirkland, C. L., Smithies, R. H., Taylor, R. J. M., Evans, N., McDonald, B., 2015. Zircon Th/U ratios in magmatic environs. Lithos. 212, 397−414.

Kobayashi, F., 2003. Palaeogeographic constraints on the tectonic evolution of the Maizuru Terrane of Southwest Japan to the eastern continental margin of South China during the Permian and Triassic. Palaeogeography, Palaeoclimatology, Palaeoecology, 195(3-4), 299-317.

Koide, T., Tazaki, K., Kagami, H., 1987. Sr isotopic study of Ibara dismembered ophiolite from

the Maizuru Tectonic Belt, southwest Japan: Journal of Japanese Association Mineralogy, Petrology and Economic Geology, 82, 1-15.

Koide, Y. 1986. Origin of the Ibara metabasalts from the Maizuru Tectonic Belt, southwest Japan. Journal of Geological Society of Japan 92, 329–48 (in Japanese with English abstract).

Kusunoki, T., Musashino, M., 1990. Permo-Triassic sandstones from the Ultra-Tamba Zone, the Tamba Belt and the Maizuru Belt-Modal composition and their composition. Earth Sci. 44, 1-11 (in Japanese with English abstract).

Kydonakis, K., Kostopoulos, D., Poujol, M., Brun, J. P., Papanikolaou, D., Paquette, J. L., 2014. The dispersal of the Gondwana Super-fan System in the eastern Mediterranean: New insights from detrital zircon geochronology. Gondwana Research, 25, 1230–1241.

Li, Y., Takeuchi, M., 2022. U–Pb dating of detrital zircon from Permian successions of the South Kitakami Belt, Northeast Japan: Clues to the paleogeography of the belt. Island Arc, 31, e12435.

Li, X. H., Li, Z. X., Li, W. X., Wang, Y., 2006. Initiation of the Indosinian Orogeny in South China: evidence for a Permian magmatic arc on Hainan Island. The Journal of geology, 114, 341-353.

Ma, Y., Zheng, D., Zhang, H., Pang, J., Wang, Y., Wu, Y., Wang, Y., He, H., 2022. Neon isotopic signature applied to detrital provenance assignment in foreland basins. Chemical Geology, 590, 120701.

Malkowski, M. A., Johnstone, S. A., Sharman, G. R., White, C. J., Scheirer, D. S., Barth, G. A., 2022. Continental shelves as detrital mixers: U–Pb and Lu–Hf detrital zircon provenance of the Pleistocene–Holocene Bering Sea and its margins. The Depositional Record , 8, 1008-1030.

Markwitz, V., Kirkland, C. L., Mehnert, A., Gessner, K., Shaw, J., 2017. 3-D characterization of detrital zircon grains and its implications for fluvial transport, mixing, and preservation bias. Geochemistry, Geophysics, Geosystems, 18, 4655–4673.

Matsuzawa, N., Takeuchi, M., 2009. Provenance and sedimentary environment of clastic rocks of the Permian accretionary complex: example of the Himekawa Complex in the Akiyoshi Belt. Abstr. 116th Annual. Mem. Geol. Soc. Japan, 409 (in Japanese).

Mavoungou, L. N., Das, K., Kawaguchi, K., Hayasaka, Y., Shibata, T., 2022. Back-arc basin closure at the East Asian margin during Permo-Triassic boundary: Evidence from geochemistry and U-Pb zircon data of sedimentary breccia from Maizuru Terrane, Southwest Japan. Geosystems and Geoenvironment, 100080.

Nagamori, H., Takeuchi, M., Furukawa, R., Nakazawa, T., Nakano, S., 2010. Geology of the Kotaki district. Quadrangle Series, 1:50,000, Geological Survey of Japan, AIST, 130p. (in Japanese with English abstract 4p.).

Nakama, T., Hirata, T., Otoh, S., Aoki, K., Yanai, S., Maruyama, S., 2010. Paleogeography of the Japanese Islands: Age spectra of detrital zircon and provenance history of the orogen. Journal of Geography. 119, 1161−1172 (in Japanese with English abstract).

Nakazawa, K., 1957. Summary of the Lower and Middle Triassic system in the Maizuru zone. The Journal of the Geological Society of Japan, 64, 125-137 (in Japanese with English abstract).

Nakazawa, T., 2001. Carboniferous reef succession of the Panthalassan open-ocean setting: example from Omi Limestone, central Japan. Facies, 44(1), 183-210.

Oh, C. W., Kusky, T., 2007. The Late Permian to Triassic Hongseong-Odesan collision belt in South Korea, and its tectonic correlation with China and Japan. International Geology Review, 49, 636-657.

Ohkawa, M., Takeuchi, M., Li, Y., Saitoh, S., Yamamoto, K., 2021. Paleogeography and tectonic evolution of a late Paleozoic to earliest Mesozoic magmatic arc in East Asia based on U-Pb ages of detrital zircons from the Early Triassic Shingai Unit, Kurosegawa Belt, Southwest Japan. Journal of Asian Earth Sciences, 212, 104724.

Ohkawa, M., Takeuchi, M., Li, Y., Yabuta, S., Yamamoto, K., 2022. Late Paleozoic to early Mesozoic tectonic evolution of Japan based on crystal morphologies and U–Pb ages of detrital zircons from the middle Permian sedimentary succession, Maizuru Belt, Southwest Japan. Journal of Asian Earth Sciences, 237, 105349.

Okawa, H., Shimojo, M., Orihashi, Y., Yamamoto, K., Hirata, T., Sano, Ishizaki., Y., Kouchi, Y., Yanai, S., Otoh, S., 2013. Detrital zircon geochronology of the Silurian–Lower Cretaceous continuous succession of the South Kitakami belt, northeast Japan. Memoir of the Fukui Prefectural Dinosaur Museum. 12, 35–78.

Ortega-Flores, B., Solari, L. A., Martini, M., 2021. Multidimensional Scaling (MDS): A quantitative approximation of zircon ages to sedimentary provenance with some examples from Mexico. Journal of South American Earth Sciences, 110, 103347.

Pastor-Galán, D., Spencer, C. J., Furukawa, T., Tsujimori, T., 2021. Evidence for crustal removal, tectonic erosion and flare-ups from the Japanese evolving forearc sediment provenance. Earth and Planetary Science Letters, 564, 116893.

Pupin, J. P., 1980. Zircon and granite petrology. Contributions to Mineralogy and Petrology, 73, 207-220.

Rubatto, D., 2017. Zircon: the metamorphic mineral. Reviews in mineralogy and geochemistry, 83, 261-295.

Rubatto, D., Hermann, J., 2003. Zircon formation during fluid circulation in eclogites (Monviso, Western Alps): implications for Zr and Hf budget in subduction zones. Geochimica et Cosmochimica Acta. 67, 2173−2187.

Sano, H., & Kanmera, K., 1988. Paleogeographic reconstruction of accreted oceanic rocks, Akiyoshi, southwest Japan. Geology, 16, 600-603.

Saylor, J.E., Jordan, J.C., Sundell, K.E., Wang, X., Wang, S. and Deng, T., 2018. Topographic growth of the Jishi Shan and its impact on basin and hydrology evolution, NE Tibetan Plateau. Basin Research, 30, 544-563.

Shen, L., Yu, J. H., O'Reilly, S. Y., Griffin, W. L., Zhou, X., 2018. Subduction-related middle Permian to early Triassic magmatism in central Hainan Island, South China. Lithos, 318, 158-175.

Shiki, T., 1962. Studies on Sandstones in the Maizuru Zone, Southwest Japan (III): Graywacke and Arkose Sandstones in and out of the Maizuru Zone. Memoirs of the College of Science, University of Kyoto. Series B, 29, 291-324.

Shimizu, D., Nakazawa, K., Shiki, T., Nogami, Y., 1962a. The Permian Maizuru Group, its stratigra¬phy and syntectonic faunal succession through the Latest Paleozoic Orogeny. Mem. Coll. Sci., Univ. Kyoto, Ser. B, 28, 571-609 (in Japanese with English abstract).

Shimizu, D., Shiki, T., Nakazawa, K., Nogami, Y., 1962b. A study on the stratigraphy and geologic structure of the Maizuru Zone (part 11); Sedimentation of the Maizuru Group and Permian tectonic movement. Jour. Geol. Soc. Japan, 68, 334-340 (in Japanese with English abstract).

Spencer, C. J., Kirkland, C. L., Taylor, R. J., 2016. Strategies towards statistically robust interpretations of in situ U−Pb zircon geochronology. Geoscience Frontiers, 7, 581−589.

Staisch, L. M., O'Connor, J. E., Cannon, C. M., Holm-Denoma, C., Link, P. K., Lasher, J., Alexander, J. A., 2022. Major reorganization of the Snake River modulated by passage of the Yellowstone Hotspot. Bulletin, 134, 1834-1844.

Suda, Y., Hayasaka, Y., Kimura, K., 2014. Crustal evolution of a Paleozoic intra-oceanic island-arc-back-arc basin system constrained by the geochemistry and geochronology of the Yakuno Ophiolite, Southwest Japan. Journal of Geological Research, 2014.

Suda, Y., Hayasaka, Y., 2009. Genesis and evolutional processes of the Paleozoic oceanic island arc crust, Asago body of the Yakuno ophiolite, southwest Japan. Journal of the Geological Society of Japan, 115, 266-287 (in Japanese with English abstract).

Suda, Y., Takeuchi, M., Kimura, K., Hayasaka, Y., 2010. SHRIMP zircon U-Pb dating of metagabbro in the Mushikawa complex, Omi area, Niigata Prefecture. Abstr. 117th Annual. Mem. Geol. Soc. Japan, 285 (in Japanese).

Sundell, K. E., Saylor, J. E., Lapen, T. J., Styron, R. H., Villarreal, D. P., Usnayo, P., Cárdenas, J., 2018. Peruvian Altiplano stratigraphy highlights along-strike variability in foreland basin evolution of the Cenozoic central Andes. Tectonics, 37, 1876-1904.

Suzuki, K., Kurihara, T., 2021. U−Pb ages and sandstone provenance of the Permian volcano-sedimentary sequence of the Hida Gaien belt, Southwest Japan: Implications for Permian sedimentation and tectonics in Northeast Asia. Journal of Asian Earth Sciences, 219, 104888.

Suzuki, S., 1992. Paleoenvironment of the 4U1ltra-Tamba zone by means of modal and chemical compositions of sandstone. Mem. Geol. Soc. Japan. 38, 71–83 (in Japanese with English abstract).

Suzuki, S., Sugita, M, Mitsuno, C., 1982. Stratigraphy and geologic structure of the Maizuru Group in the Maizuru area, Southwest Japan. The Journal of the Geological Society of Japan, 88, 835-848 (in Japanese with English abstract).

Taira, A., 2001. Tectonic evolution of the Japanese island arc system. Annual Review of Earth and Planetary Sciences, 29, 109-134.

Takagi, H., Arai, H., 2003. Restoration of exotic terranes along the Median Tectonic Line, Japanese Islands: overview. Gondwana Research, 6, 657-668.

Takeuchi, M., Kawai, M., Matsuzawa, N., 2008. Detrital garnet and chromian spinel chemistry of Permian clastics in the Renge area, central Japan: Implications for the paleogeography of the East Asian continental margin. Sedimentary Geology, 212, 25-39.

Tanaka, T., Hara, A., Ohba, T., Kiminami, K., 1987. Stratigraphy, geologic structure and sedimentary environment of the Permian Nishiki Group in the Sangun-Chugoku Belt, Southwest Japan (Preliminary report). Chikyu-Kagaku, 41, 182-187 (in Japanese).

Tazawa J., Aita Y., Yuki T., Otsuki K., 1984. Discovery of Permian radiolarians from the "non-calcareous Paleozoic strata" of Omi, Central Japan, Earth Science (Chikyu Kagaku), 38, 264-267 (in Japanese).

Tazawa, J. I., Fujikawa, M., Ota, Y., 2009. Permian brachiopods from the Tsunemori Formation of the Akiyoshi area, southwest Japan: Fossil evidence for the accretion site of the Akiyoshi Terrane. Jour. Geol. Soc. Japan, 115, 168-176.

Tietz, O., 2003. Zircon typological investigations from the Seufzergründel placer near Hermsdorf in the Saxon Switzerland, Eastern Germany. GeoLines, 15, 160-167.

Tsujimori, T., Liou, J. G., Ernst, W. G., Itaya, T., 2006. Triassic paragonite-and garnet-bearing epidote-amphibolite from the Hida Mountains, Japan. Gondwana Research, 9, 167-175.

Tsutsumi, Y., Yokoyama, K., Terada, K., Sano, Y., 2000. SHRIMP U-Pb dating of zircons in the sedimentary rocks from the Akiyoshi and Suo zones, Southwest Japan. Journal of Mineralogical and Petrological Sciences, 95, 216-227.

Tsutsumi, Y., Yokoyama, K., Kasatkin, S. A., Golozubov, V. V., 2014. Zircon U−Pb age of granitoids in the Maizuru Belt, southwest Japan and the southernmost Khanka Massif, Far East Russia. Journal of Mineralogical and Petrological Sciences, 109, 97−102.

Tsutsumi, Y., Yokoyama, K., Terada, K., Sano, Y., 2000. SHRIMP U-Pb dating of zircons in the sedimentary rocks from the Akiyoshi and Suo zones, Southwest Japan. Journal of Mineralogical and Petrological Sciences, 95, 216-227.

Tokiwa, T., Shimura, Y., Takeuchi, M., Shimosato, S., Yamamoto, K., Mori, H., 2019. Provenance of trench-fill deposits of the Jurassic Chichibu accretionary complex, Southwest Japan. Journal of Asian Earth Sciences, 184, 103970.

Ujihara, M., 1985. Permian olistostrome and clastic rocks in the Himekawa area, northeast Hida Marginal Belt. Joetsu and Ashio Belts, 2, 159-168 (in Japanese).

Vermeesch, P., 2013. Multi-sample comparison of detrital age distributions. Chemical Geology, 341, 140-146.

Wakita, K., 2013. Geology and tectonics of Japanese islands: a review−the key to understanding the geology of Asia. Journal of Asian Earth Sciences, 72, 75-87.

Wakita, K., Miyazaki, K., Toshimitsu, S., Yokoyama, S. Nakagawa, M., 2007. Geology of the Ino district. Quadrangle Series, 1 : 50,000, Geological Survey of Japan, AIST, p. 140 (in Japanese with English abstract).

Wakita, K., Yoshida, R., Fushimi, Y., 2018. Tectonic setting for Tsunemori Formation in the Permian accretionary complex of the Akiyoshi Belt, Southwest Japan. Heliyon, 4, e01084.

Wang, C., Liang, X., Xie, Y., Tong, C., Pei, J., Zhou, Y., Jiang, Y., Fu, J., Dong, C., Liu, P., 2014. Peovenance of Upper Miocene to Quaternary sediments in the Yinggehai−Song Hong Basin, South China Sea: Evidence from detrital zircon U−Pb ages. Marine Geol, 355, 202−217.

Wen, F., Tian, Z., Liu, P. H., Xu, W., Liu, F., Mitchell, R. N., 2021. Sedimentary evidence for the early Paleoproterozoic tectono-magmatic lull: Detrital zircon provenance of the 2.47–2.17 Ga Langzishan Formation, Liaohe Group, Eastern Block of the North China Craton. Journal of Asian Earth Sciences, 221, 104939.

Xu, J., Xia, X. P., Lai, C., Long, X., Huang, C., 2019. When did the Paleotethys Ailaoshan

Ocean close: New insights from detrital zircon U-Pb age and Hf isotopes. Tectonics, 38, 1798-1823.

Yamasaki, T., 2020. The~ 500 Ma Asaji ultramafic–mafic intrusion in Kyushu, southwest Japan: Implications for boninitic magmatism in a late Cambrian nascent arc. Journal of Asian Earth Sciences, 188, 104107.

Yang, H., Ge, W., Dong, Y., Bi, J., Wang, Z., Ji, Z., Yang, H., Ge, W. C., Dong, Y., Bi, J. H., Wang, Z. H., Ji, Z., 2017. Record of Permian–Early Triassic continental arc magmatism in the western margin of the Jiamusi Block, NE China: Petrogenesis and implications for Paleo-Pacific subduction. International Journal of Earth Sciences, 106, 1919-1942.

Yang, H., Ge, W., Zhao, G., Yu, J., Zhang, Y., 2015. Early Permian–Late Triassic granitic magmatism in the Jiamusi–Khanka Massif, eastern segment of the Central Asian Orogenic Belt and its implications. Gondwana Research, 27, 1509-1533.

Yao, W. H., Li, Z. X., Li, W. X., Li, X. H., Yang, J. H., 2014. From Rodinia to Gondwanaland: A tale of detrital zircon provenance analyses from the southern Nanhua Basin, South China. American Journal of Science, 314, 278-313.

Yi, K., Cheong, C. S., Kim, J., Kim, N., Jeong, Y. J., Cho, M., 2012. Late Paleozoic to Early Mesozoic arc-related magmatism in southeastern Korea: SHRIMP zircon geochronology and geochemistry. Lithos, 153, 129-141.

Yoshida, K. Tazawa, J., 2000. The sedimentary system and the tectonic implication of the Usugimu–type conglomerate in the South Kitakami Terrane, northeast Japan:especially to the sandstone petrography and the sedimentary facies of the Middle Permian coarse clastic deposits. Jour. Geol. Soc. Japan, 56, 89–102 (in Japanese with English Abstract).

Yoshida, K., Machiyama, H., 2004. Provenance of Permian sandstones, South Kitakami terrane, northeast Japan: implications for Permian arc evolution. Sedimentary Geology, 166, 185−207.

Yue, Y., Graham, S. A., Ritts, B. D., Wooden, J. L., 2005. Detrital zircon provenance evidence for large-scale extrusion along the Altyn Tagh fault. Tectonophysics, 406, 165-178.

Zeh, A., Cabral, A. R., 2021. Combining detrital zircon shape and U–Pb–Hf isotope analyses for provenance studies–An example from the Aquiri region, Amazon Craton, Brazil. Precambrian Research, 364, 106343.

Zeh, A., Wilson, A. H., 2022. U-Pb-Hf isotopes and shape parameters of zircon from the Mozaan Group (South Africa) with implications for depositional ages, provenance and Witwatersrand–Pongola Supergroup correlations. Precambrian Research, 368, 106500.

Zhang, X., Takeuchi, M., Lee, H. Y., 2019. Tracing the origin of Southwest Japan using the Hf

isotopic composition of detrital zircons from the Akiyoshi Belt. Terra Nova, 31, 11-17.

Zhang, X., Takeuchi, M., Ohkawa, M., Matsuzawa, N., 2018a. Provenance of a Permian accretionary complex (Nishiki Group) of the Akiyoshi Belt in southwest Japan and paleogeographic implications. Journal of Asian Earth Sciences, 167, 130-138.

Zhang, X., Xu, W., Sun, C., Xu, T., Wang, F., 2018b. Crustal accretion and reworking within the Khanka Massif: Evidence from Hf isotopes of zircons in Phanerozoic granitoids. Journal of Earth Science, 29, 255-264.

Zieger, J., Rothe, J., Hofmann, M., Gärtner, A., Linnemann, U., 2019. The Permo-Carboniferous Dwyka Group of the Aranos Basin (Namibia)−How detrital zircons help understanding sedimentary recycling during a major glaciation. Journal of African Earth Sciences, 158, 103555.

Zoleikhaei, Y., Frei, D., Morton, A., Zamanzadeh, S. M., 2016. Roundness of heavy minerals (zircon and apatite) as a provenance tool for unraveling recycling: A case study from the Sefidrud and Sarbaz rivers in N and SE Iran. Sedimentary Geology, 342, 106-117.

Figures and Tables
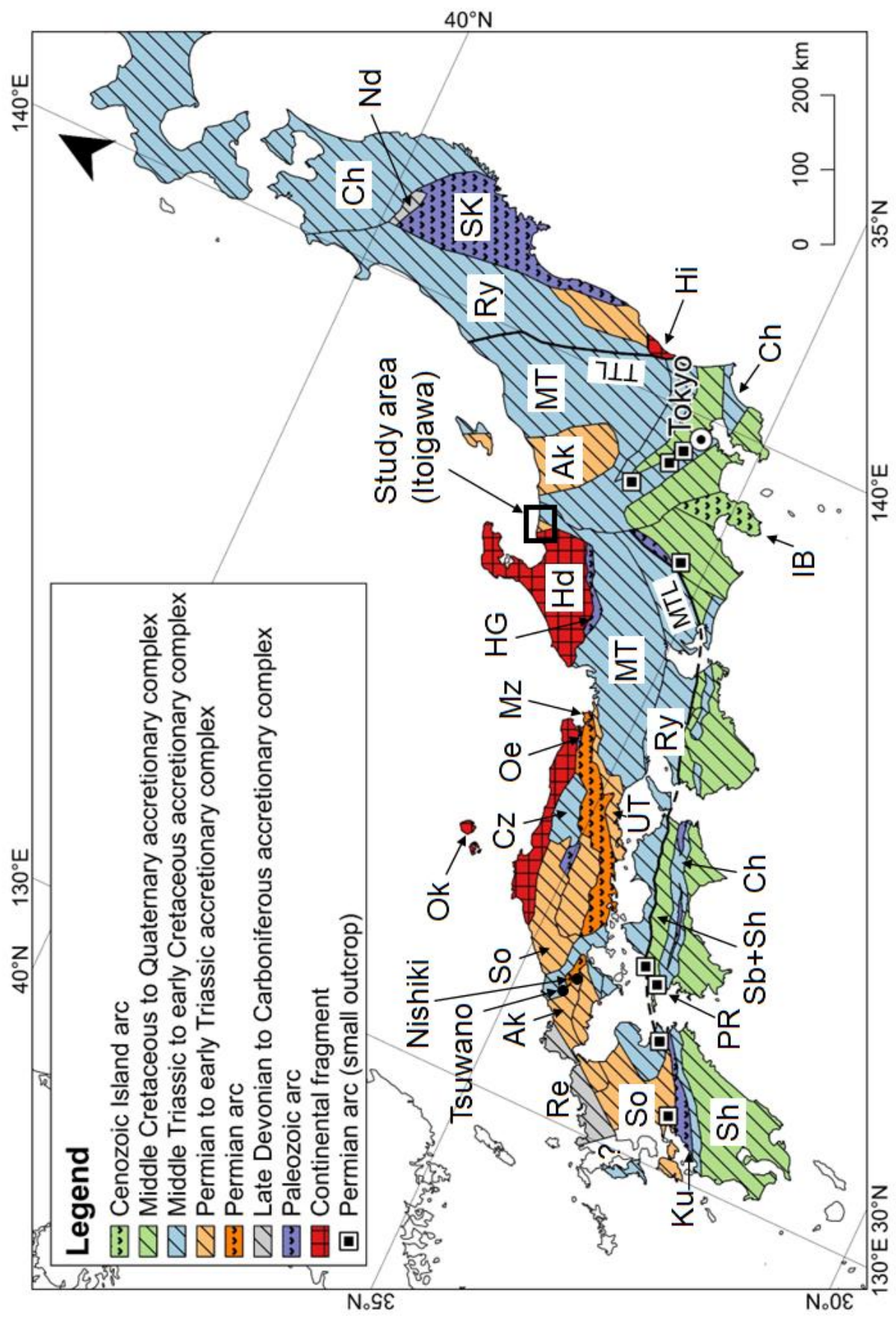
Fig. 1　Tectonic map of Japanese islands based on public domain Natural Earth data (modified from Takagi and Arai, 2003; Isozaki et al., 2010; Wakita et al., 2013). MTL: Median tectonic line, TTL: Tanakura tectonic line, AK: Akiyoshi Belt, Ch: Chichibu Belt, Cz: Chizu Belt, Hd: Hida Belt, HG: Hida-Gaien Belt, Hi: Hitachi Belt, IB: Izu-Bonin Arc, Ks: Kurosegawa Belt, MT: Mino-Tamba Belt, Mz: Maizuru Belt, Nd: Nedamo Belt, Oe: Oeyama Ophiolite, Ok: Oki Belt, Re: Renge Belt, Ry: Ryoke Belt, Sb: Sanbagawa Belt, SK: South Kitakami Belt, Sh: Shimanto Belt, So: Suo Belt, UT: Ultra-Tamba Belt.
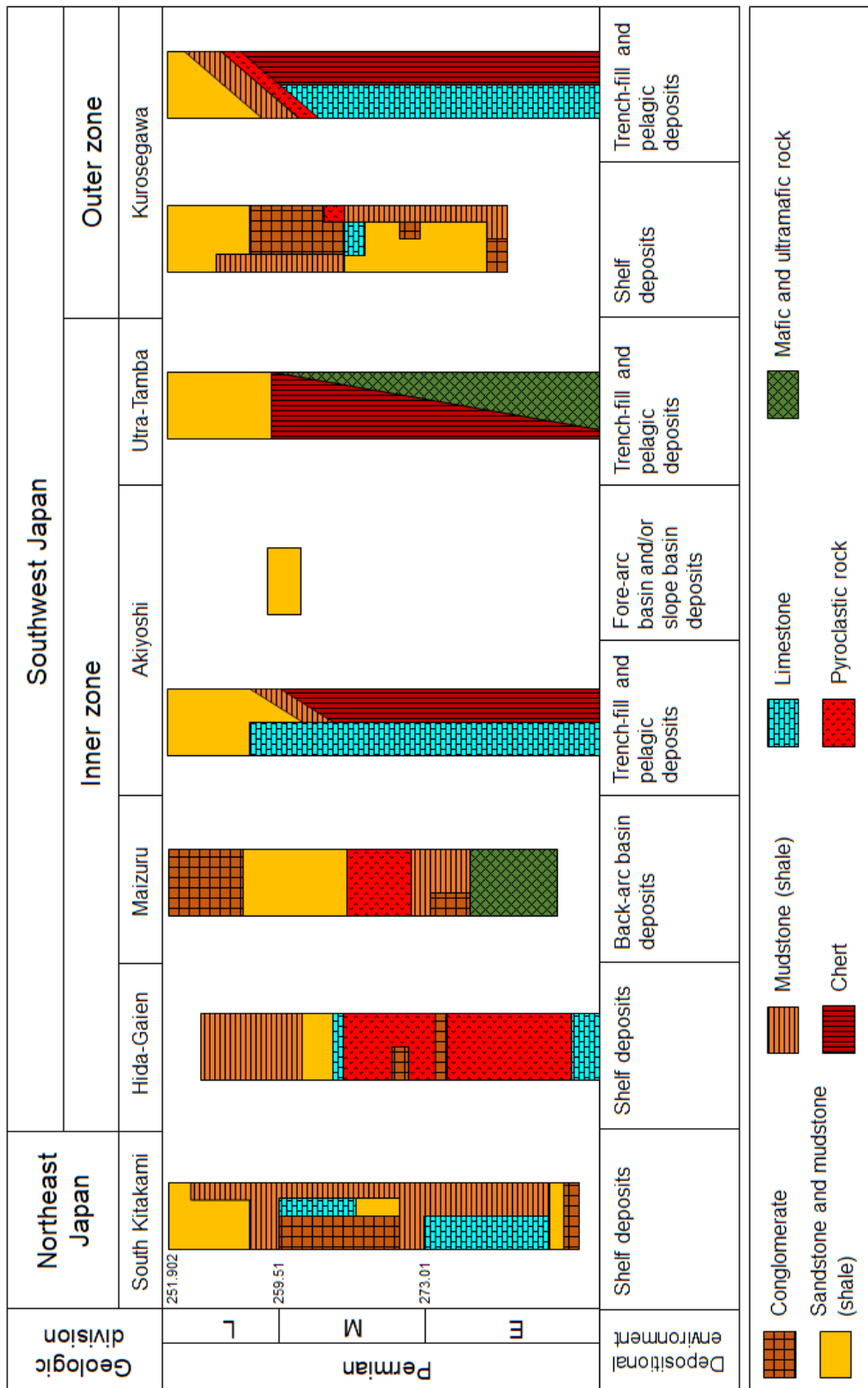
Fig. 2　Simplified columnar sections of Permian strata in Japan and their depositional environments (modified from Isozaki, 1986; Hayasaka, 1996; Ehiro, 2000, 2001, 2017; Wakita et al., 2007, 2018; Takeuchi et al., 2008; Okawa et al., 2013; Hara et al., 2014; Suzuki and Kurihara, 2021).
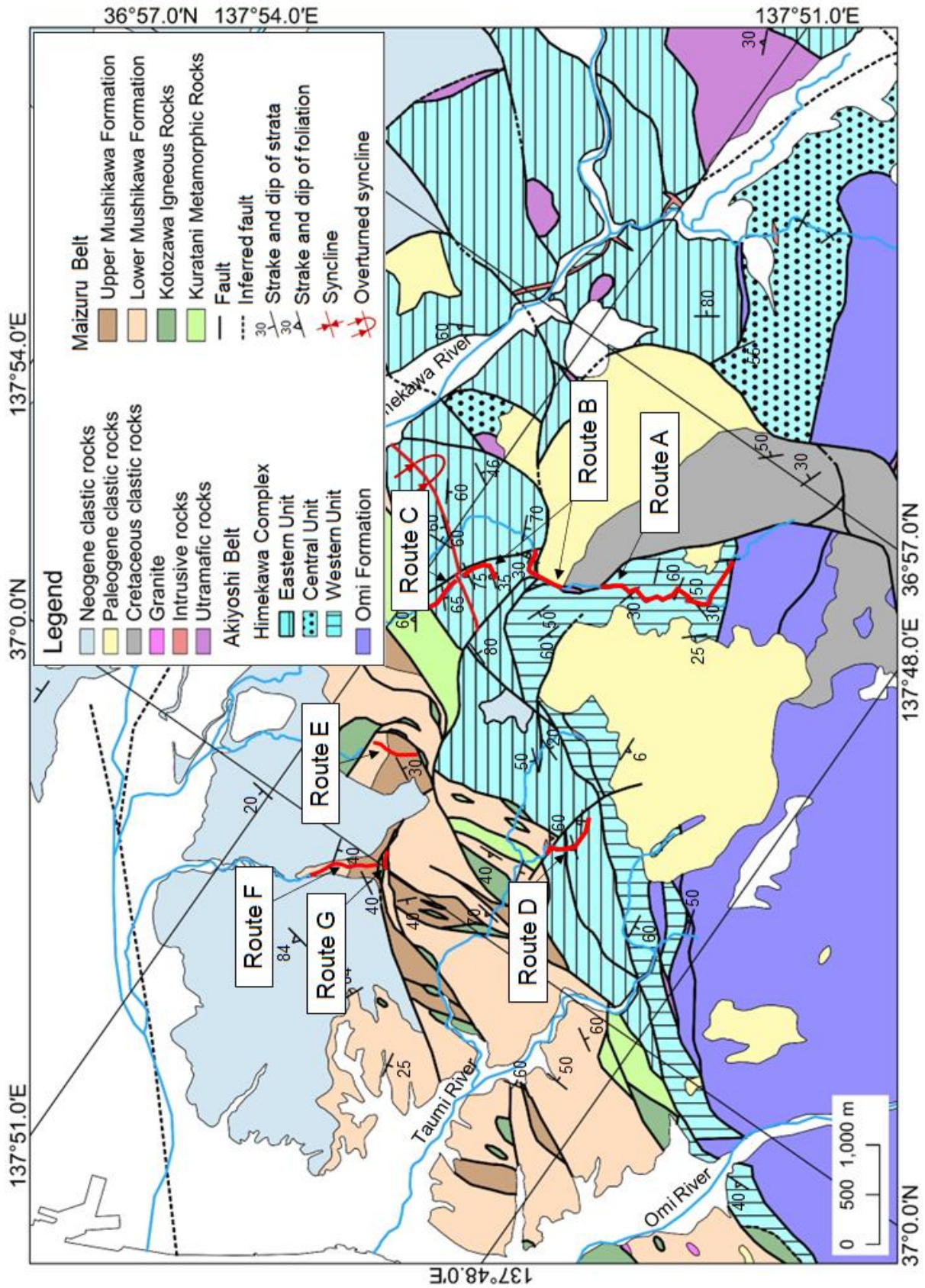
Fig. 3   Geological map of Itoigawa area, Niigata prefecture (after Nagamori et al., 2010; Ohkawa et al., 2022). The location of the Itoigawa area is shown in Fig. 1.
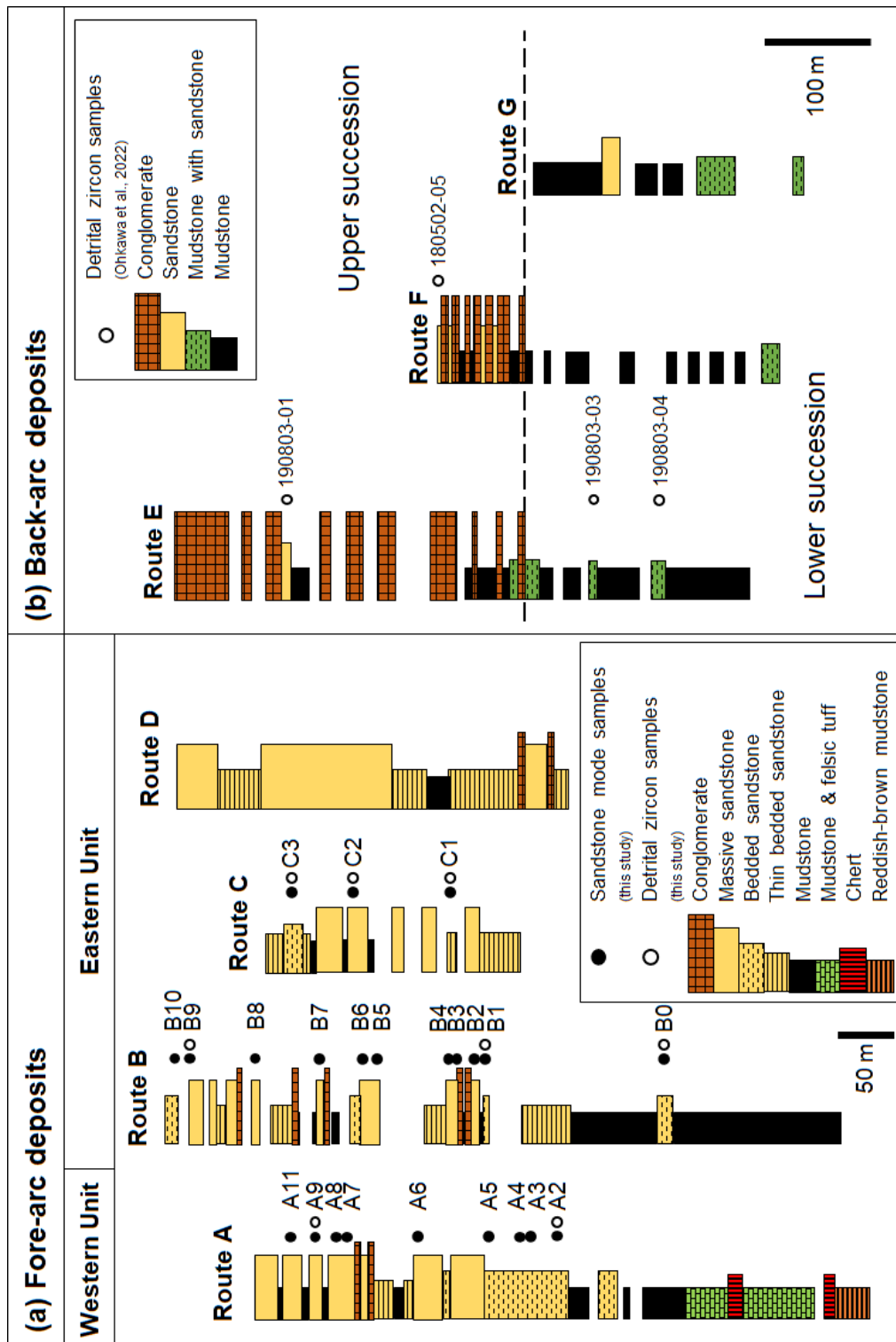
Fig. 4   (a) Geological columnar sections in Permian fore-arc deposits (Himekawa Complex of Akiyoshi Belt) (modified from Takeuchi et al., 2008; Nagamori et al., 2010). (b) Geological columnar sections in Permian back-arc deposits (Mushikawa Formation of Maizuru Belt) (modified from Nagamori et al., 2010; Ohkawa et al., 2022). The location of each columnar section number is shown in Fig. 3.
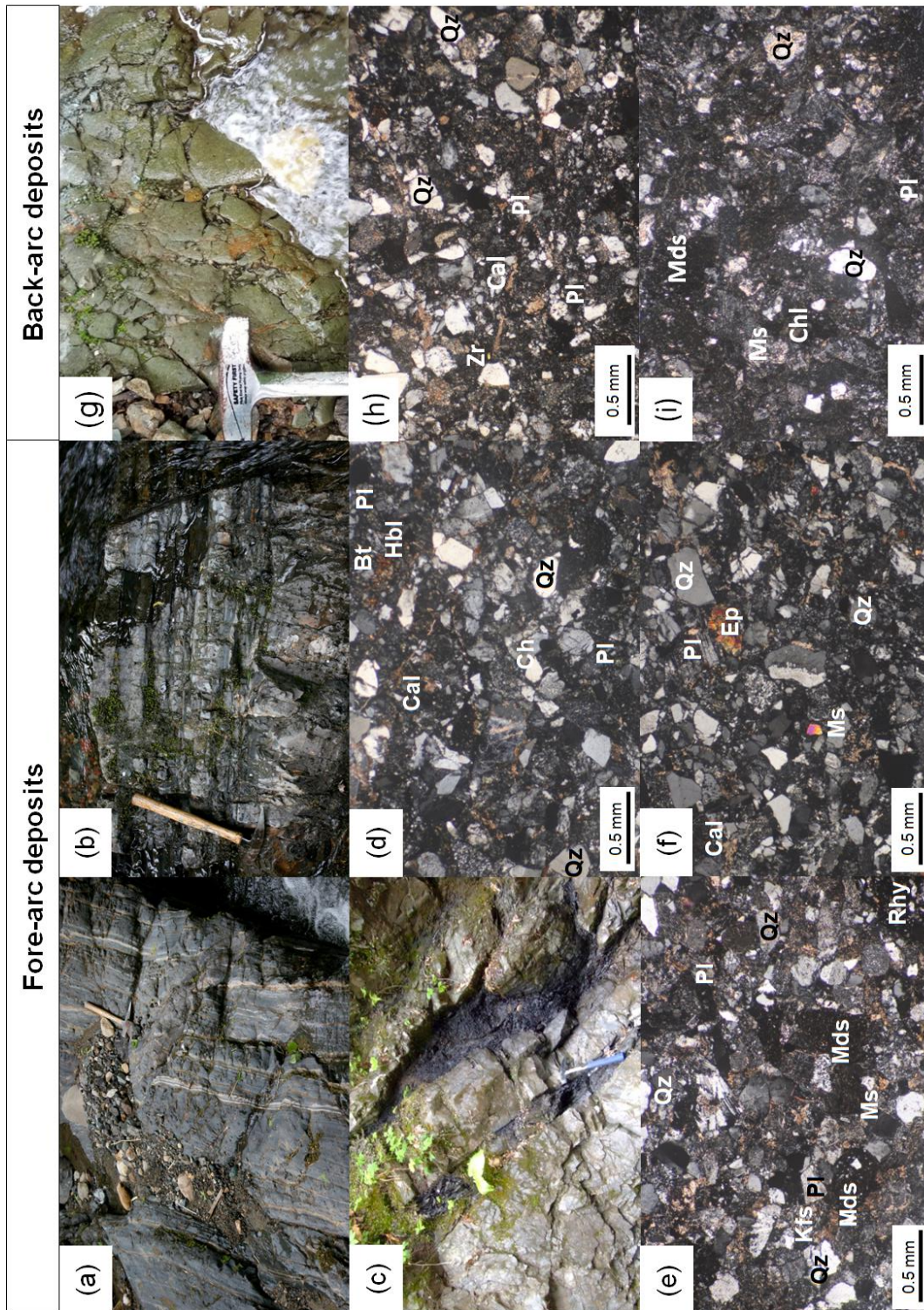
Fig. 5　Field photographs (a, b, c, g) and cross-polarized light photomicrographs of thin sections from sandstones (d, e, f, h, i) in the fore- and back-arc deposits, Itoigawa area (after Ohkawa et al., 2022). (a) Alternating beds of siliceous tuff and mudstone in Western Unit. (b) Tin bedded sandstone in Eastern Unit. (c) Massive sandstone in Eastern Unit. (d) Sample A9. (e) Sample B1. (f) Sample C2. (g) Sandstone of the lower succession. (h) Sample 190803-3. (h) Sample 190803-1. Qz: quartz, Pl: plagioclase, Kfs: K-feldspar, Bt: biotite, Cal: calcite, Chl:

Chlorite, Hbl: hornblende, Ep: epidote, Zr: zircon, Ms: muscovite, Rhy: rhyolitic rock, Hf: hornfels, Mds: mudstone. The lengths of the hammers are 24 (a, b) and 33 cm (c, g).
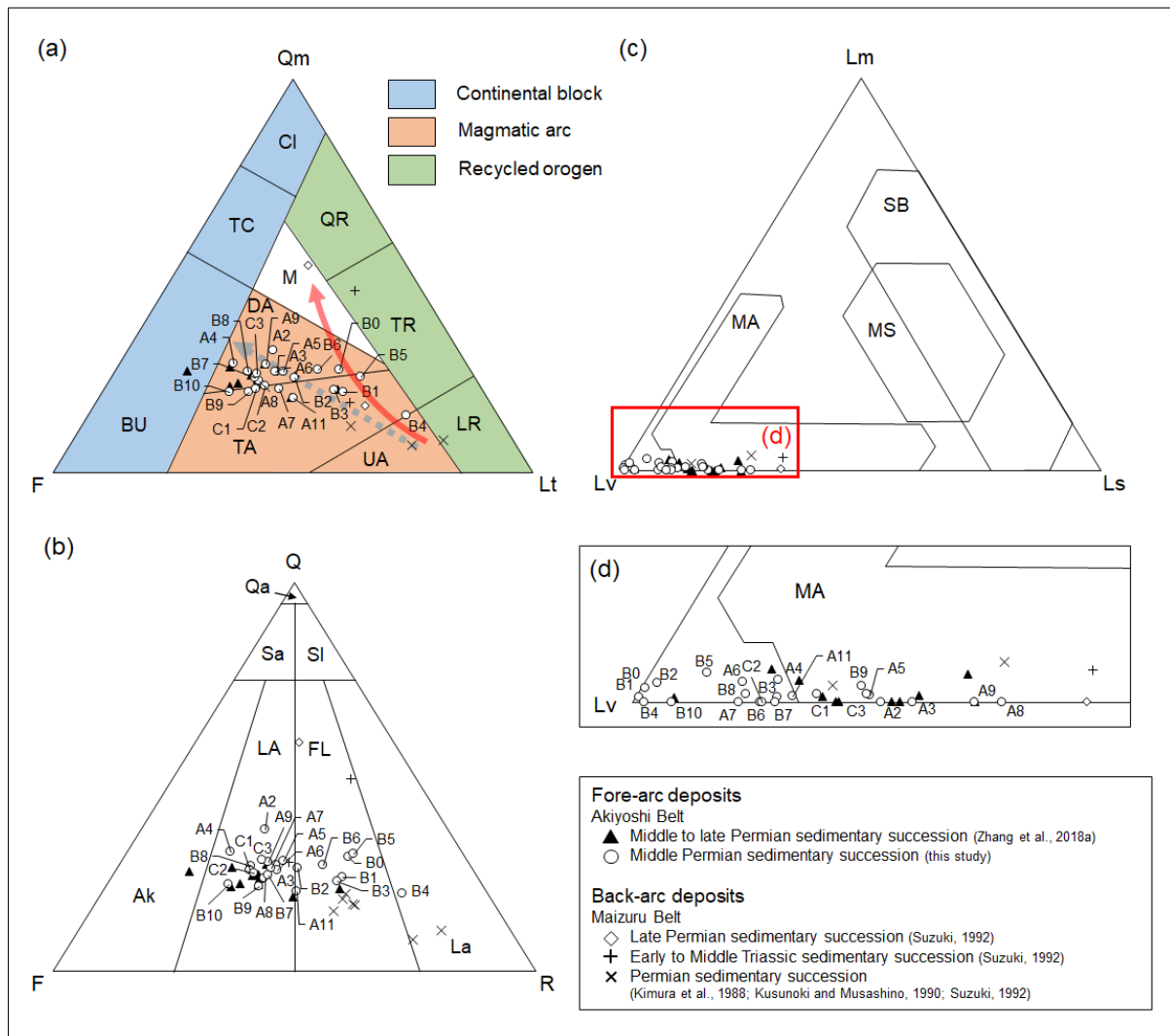
Fig. 6   Qm–F–Lt (a), Q–F–R (b), and Lm–Lv–Ls (c) plots from the sandstones in the fore- and back-arc deposits (Folk, 1968, 1980; Ingersoll and Suczek, 1979; Dickinson, 1985; Kimura et al., 1988; Kusunoki and Musashino, 1990; Suzuki, 1992; Zhang et al., 2018a; this study). A gray dashed line indicates increasing of the ratio of plutonic to volcanic sources (Dickinson, 1985). A solid red line indicates the trend of the Permian to Triassic sandstone composition changes of the Maizuru Belt. Qm: monocrystalline quartz, F: total feldspar grains, Lt: lithic fragments+polycrystalline quartz, Q: total quartz grains, F: total feldspar grains, R: total rock fragments, Lm metamorphic lithic fragments, Lv: volcanic lithic fragments, Ls: sedimentary lithic fragments, CI: cratonic interior, BU: basement uplift, DA: dissected arc, LR: lithic recycled, M: mixed, QR: quartzose recycled, TA: transitional arc, TC: transitional continental, TR: transitional recycled, UA: undissected arc, Qa: quartzarenite, Sa: subarkose, Sl: sublitharenite, Ak: arkose, LA: lithic arkose, FL: Feldspathic litharenite, La: litharenite, MA: magmatic arc, MS: mixed magmatic arc & subduction complex, SB: suture belts.
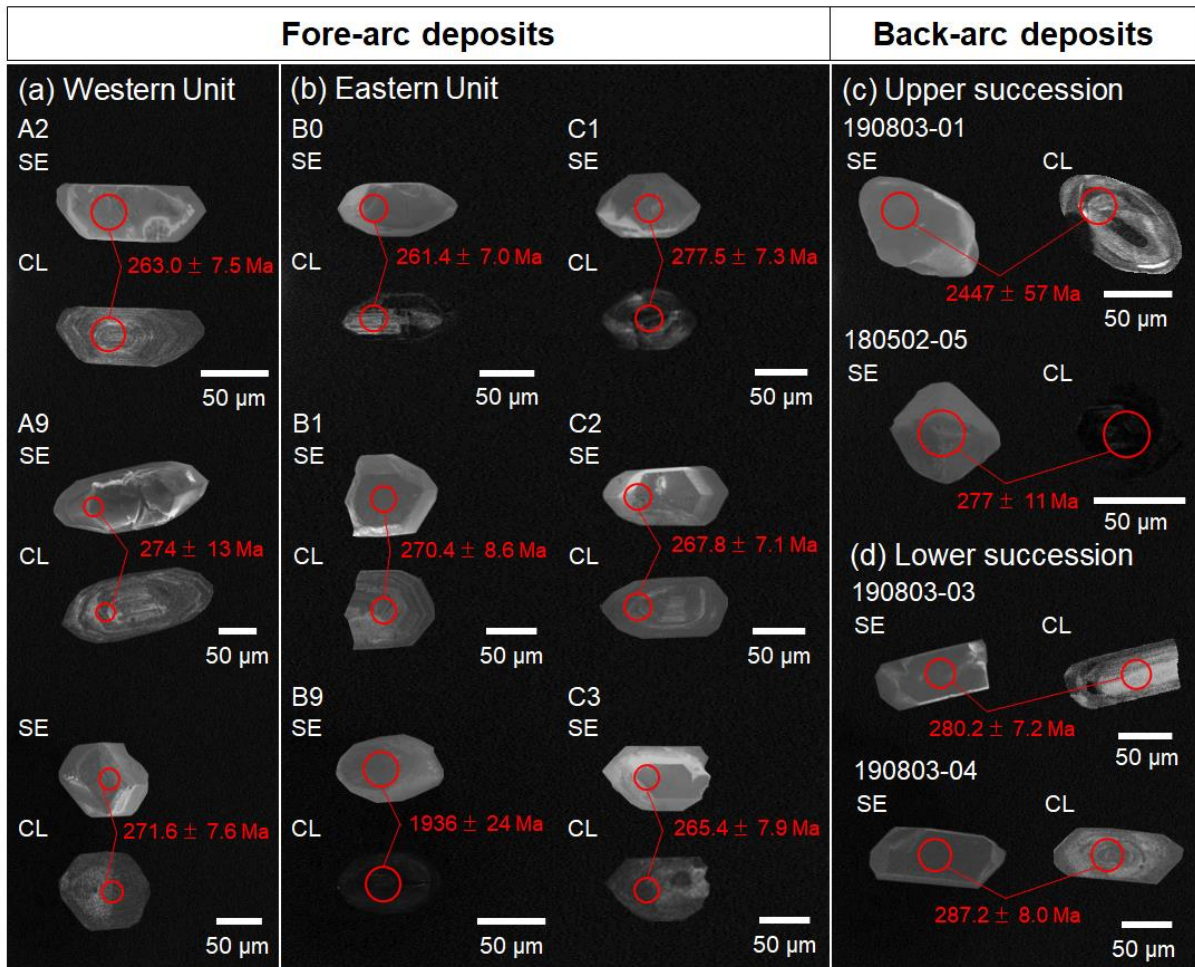
Fig. 7　Secondary electron (SE) and cathodoluminescence (CL) images of selected zircons from sandstones in the fore- and back-arc deposits, Itoigawa area (Ohkawa et al., 2022; this study). Red circles and parentheses show the locations of analysis spots. (a) Western Unit. (b) Eastern Unit. (c) Upper succession. (d) Lower succession.
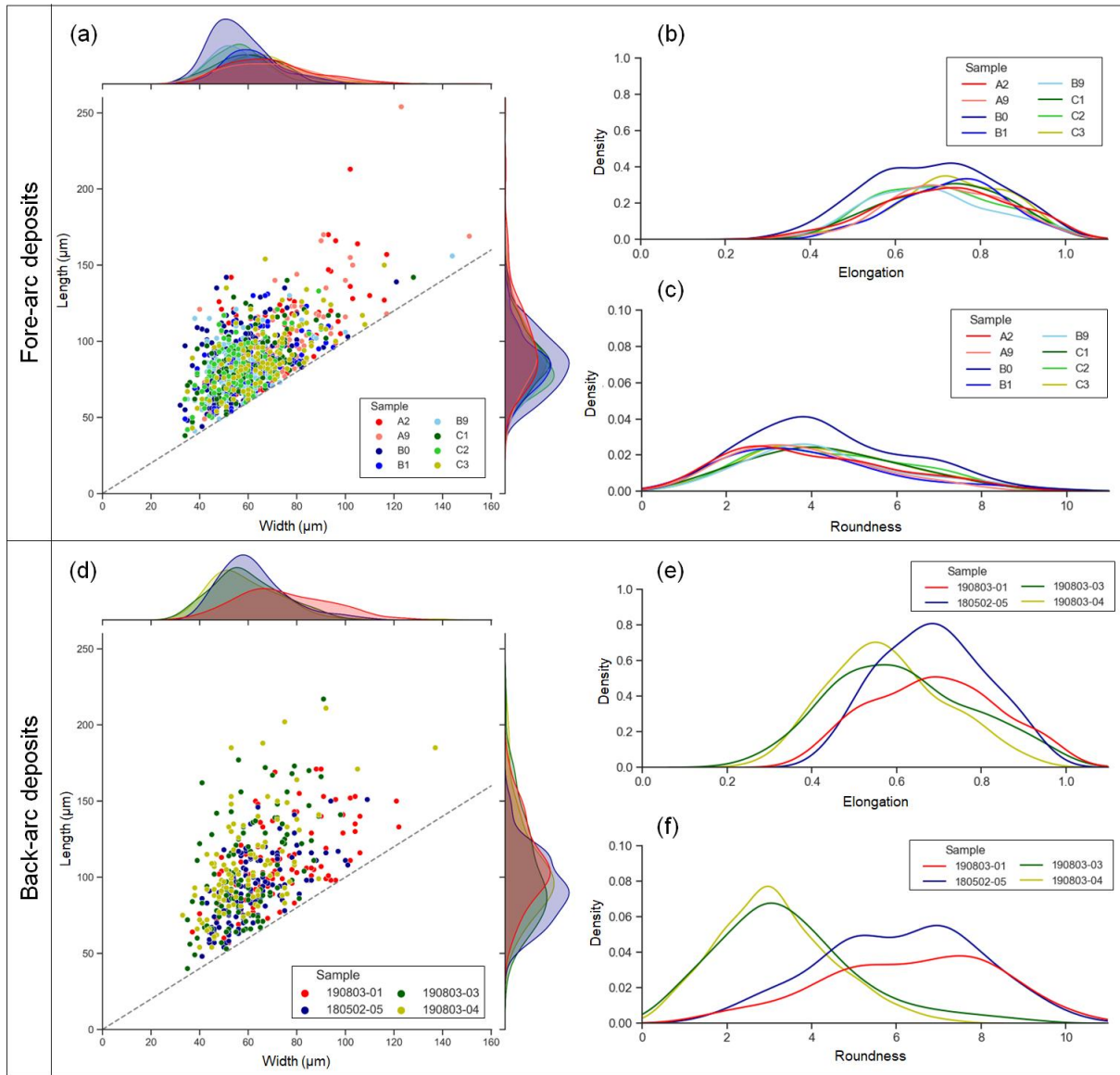
Fig. 8   Scatter plot and kernel density estimations of length and width (a, d) and kernel density estimations of elongation (b, e) and roundness (c, f) for detrital zircons from sandstones in the fore- and back-arc deposits, Itoigawa area (Ohkawa et al., 2022; this study). A gray dashed line shows a 1:1 reference line between length and width for detrital zircons.

Fig. 9 Morphotype classification for detrital zircons from sandstones in the fore- and back-arc deposits, Itoigawa area (Ohkawa et al., 2022; this study). Values indicate the number of each morphotype. (a) Western Unit. (b) Eastern Unit. (c) Upper succession. (d) Lower succession.
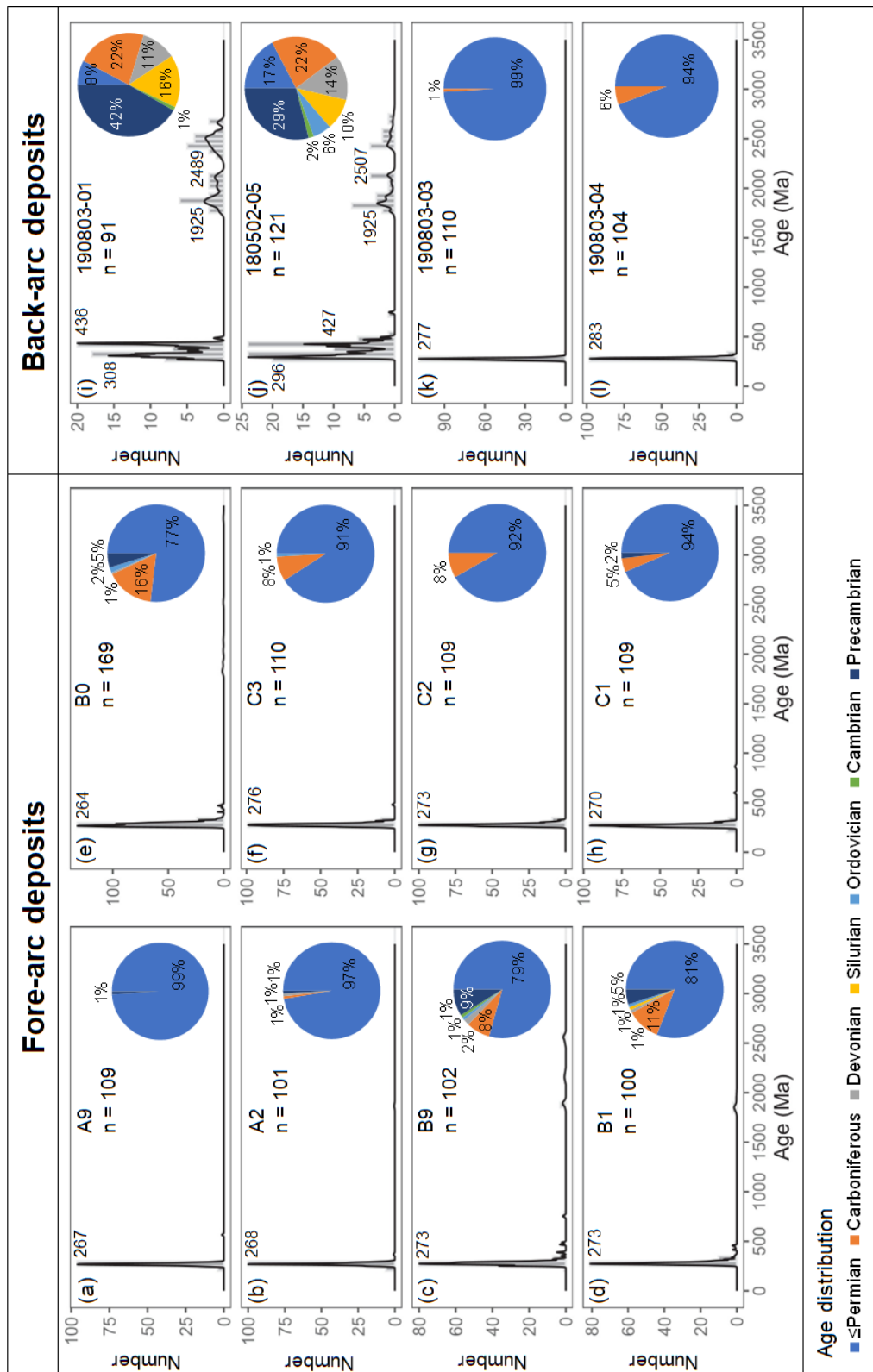
Fig. 10　Relative probability density plots for detrital zircons from sandstones in the fore- and back-arc deposits, Itoigawa area (Ohkawa et al., 2022; this study). Values of the graphs indicate the main age clusters. (a) A9. (b) A2. (c) B9. (d) B1. (e) B0. (f) C3. (g) C2. (h) C1. (i) 190803-01. (j) 180502-05. (k) 190803-03. (l) 190803-04.
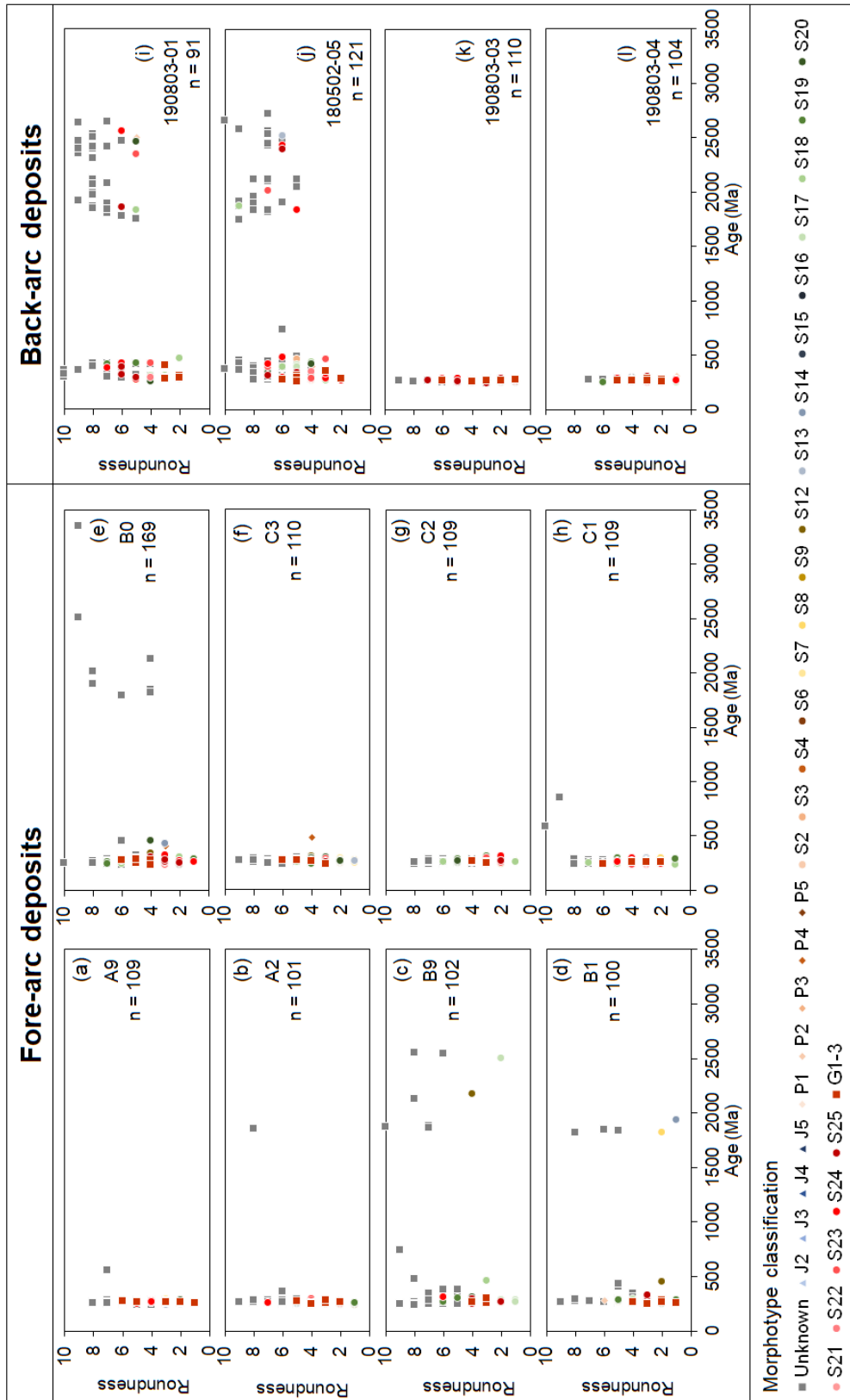
Fig. 11 (a) Relationship among U–Pb ages, roundness values, and morphotypes for detrital zircons from sandstones in the fore- and back-arc deposits, Itoigawa area (Ohkawa et al., 2022; this study). (a) A9. (b) A2. (c) B9. (d) B1. (e) B0. (f) C3. (g) C2. (h) C1. (i) 190803-01. (j) 180502-05. (k) 190803-03. (l) 190803-04.
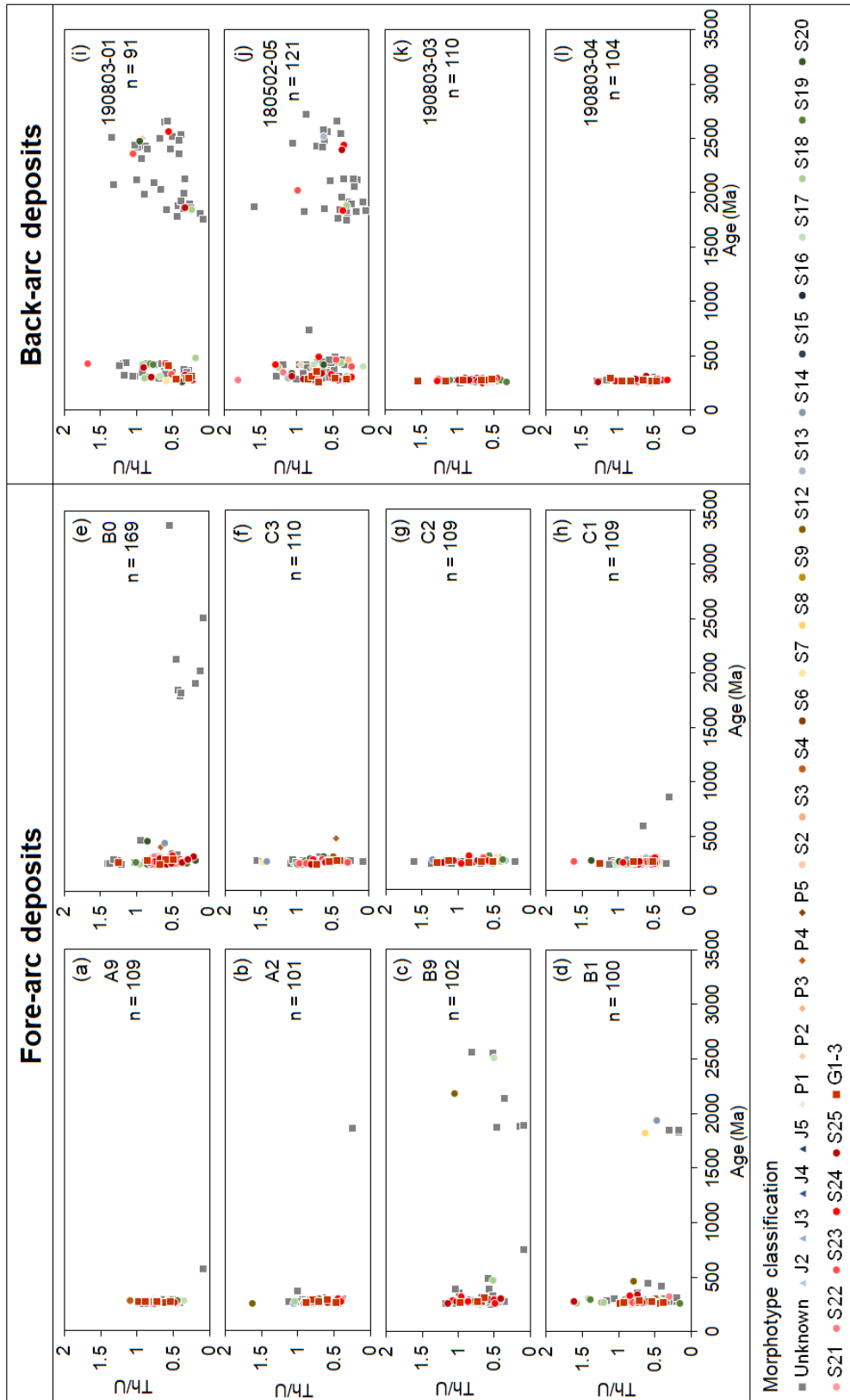
Fig. 12 Relationship among U–Pb ages, Th/U ratios, and morphotypes for detrital zircons from sandstones in the fore- and back-arc deposits, Itoigawa area (Ohkawa et al., 2022; this study). (a) A9. (b) A2. (c) B9. (d) B1. (e) B0. (f) C3. (g) C2. (h) C1. (i) 190803-01. (j) 180502-05. (k) 190803-03. (l) 190803-04.
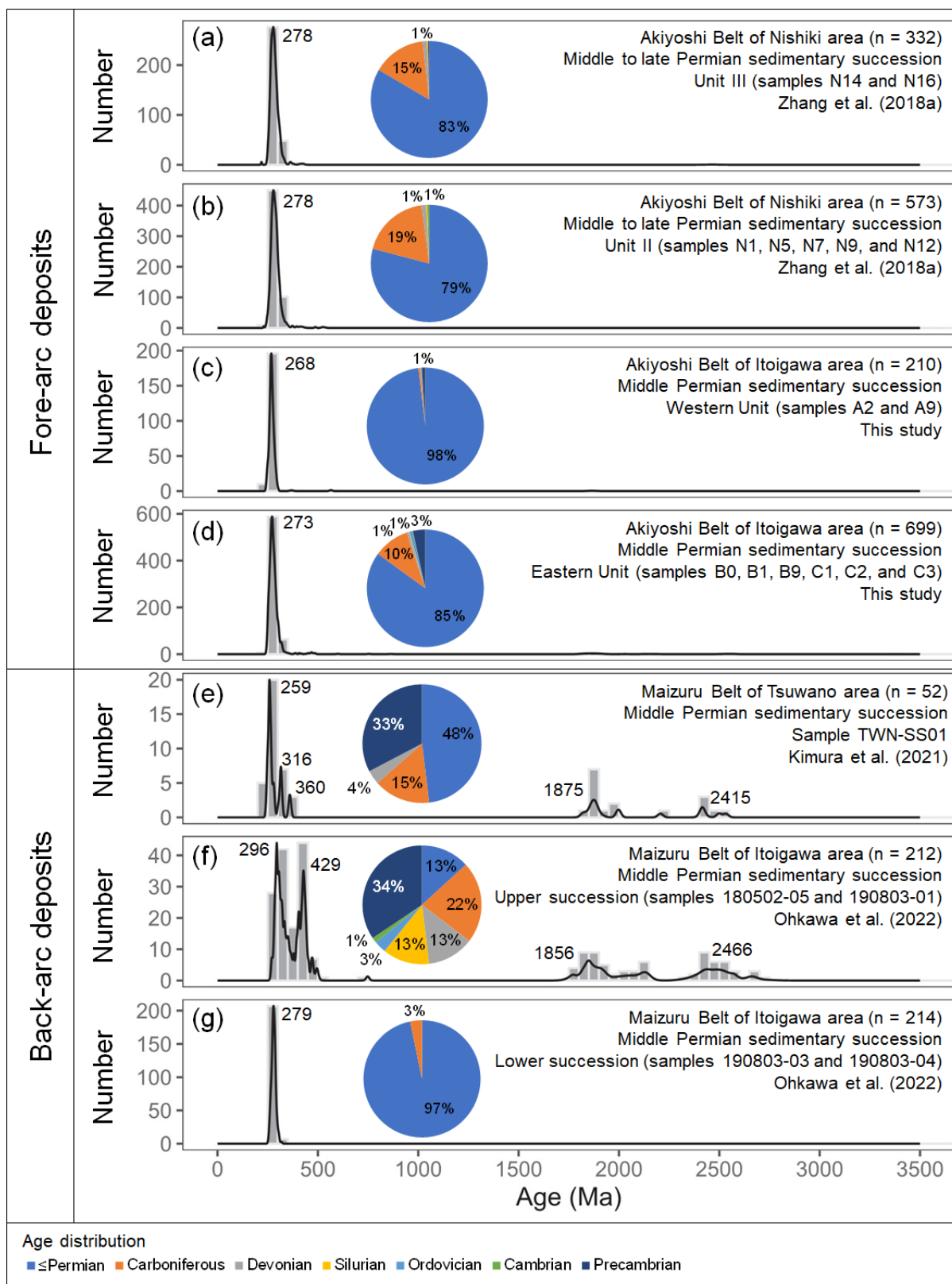
Fig. 13 Relative probability density plots for detrital zircons from Permian fore- and back-arc deposits (Zhang et al., 2018a; Kimura et al., 2021; Ohkawa et al., 2022; this study). Values in the plots indicate main age clusters.

49
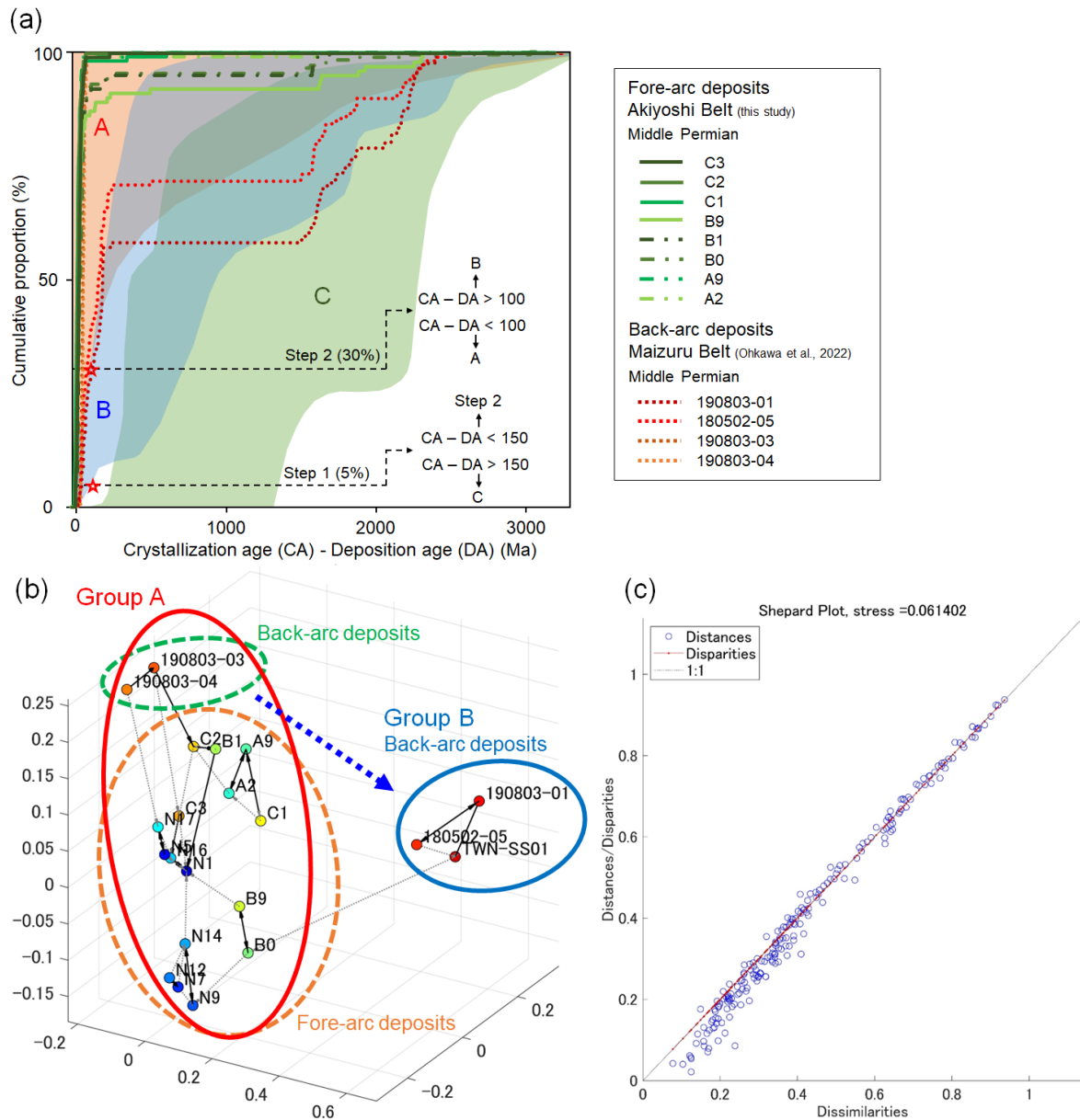
Fig. 14 (a) Cumulative proportion plots of difference between crystallization–deposition ages from Permian fore- and back-arc deposits (modified from Cawood et al., 2012; Ohkawa et al., 2022; this study). A: convergent setting, B: collisional setting, C: extensional setting. (b) MDS plot (Vermeesch, 2013) for detrital U–Pb ages from Permian fore- and back-arc deposits (Zhang et al., 2018a; Kimura et al., 2021; Ohkawa et al., 2022; this study). Solid and dashed lines indicate the closest and second-closest neighbors, respectively. A blue dashed line indicates the trend of MDS plot variation of back-arc deposits. (c) Shepard plot of the MDS map (after Vermeesch, 2013).
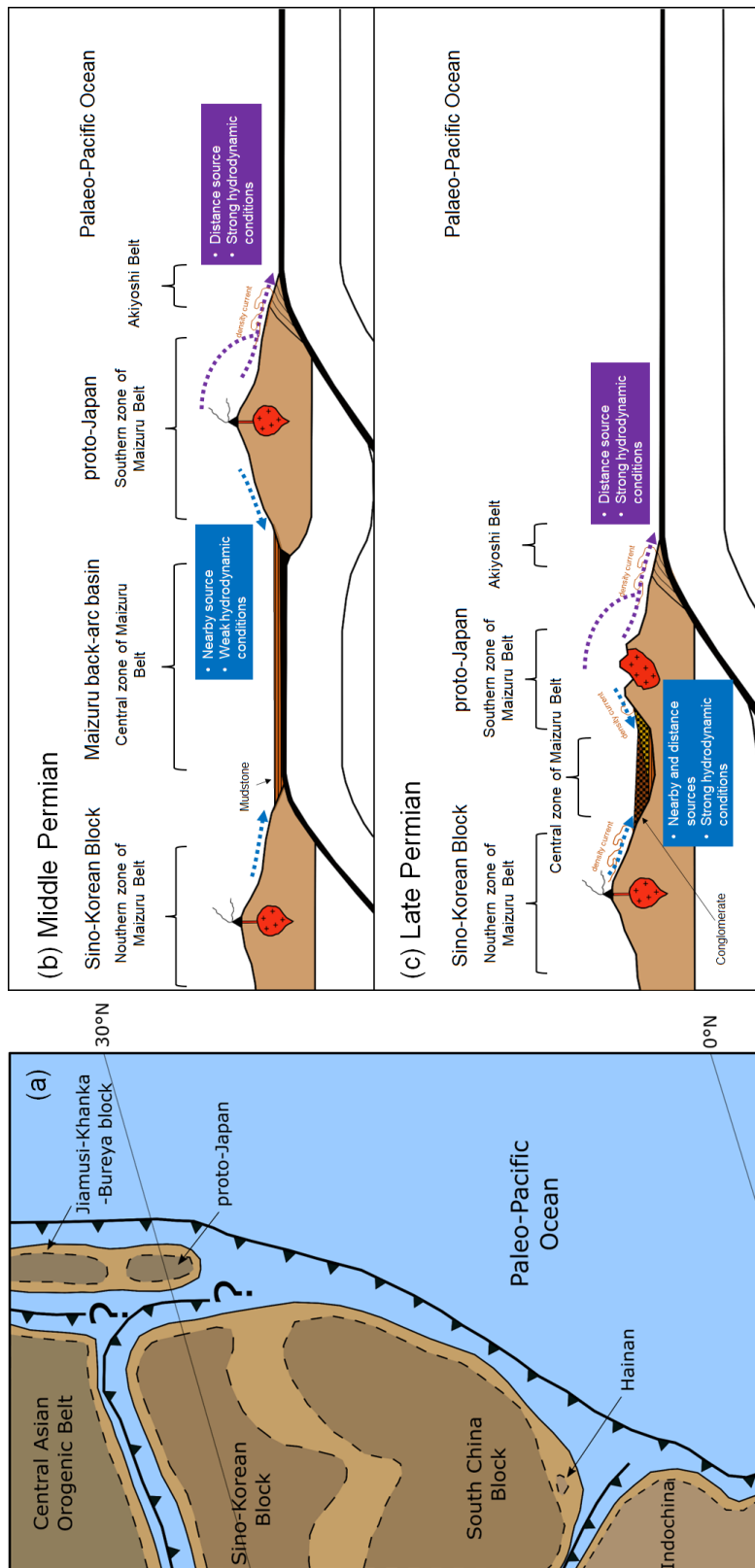
Fig. 15 Middle Permian plate reconstruction model of proto-Japan and East Asia (a) (modified from de Jong et al., 2009; Ohkawa et al., 2022), and middle Permian (b) and late Permian (c) conceptual model of tectonic evolution in proto-Japan and East Asia (modified from de Jong et al., 2009; Ohkawa et al., 2021, 2022; Mavoungou et al., 2022).

Table 1 Summary of published and new measured detrital zircon data from Permian fore- (Akiyoshi Belt) and back-arc (Maizuru Belt) deposits (Zhang et al., 2018a; Kimura et al., 2021; Ohkawa et al., 2022; this study). The location of each area is shown in Fig. 1.

Tectonic Belt	Location	Depositional environment	Age	Sample name	Reference
Akiyoshi Belt	Nishiki	Trench-fill and pelagic deposits	Middle to late Permian	N1	Zhang et al. (2018a)
Akiyoshi Belt	Nishiki	Trench-fill and pelagic deposits	Middle to late Permian	N5	Zhang et al. (2018a)
Akiyoshi Belt	Nishiki	Trench-fill and pelagic deposits	Middle to late Permian	N7	Zhang et al. (2018a)
Akiyoshi Belt	Nishiki	Trench-fill and pelagic deposits	Middle to late Permian	N9	Zhang et al. (2018a)
Akiyoshi Belt	Nishiki	Trench-fill and pelagic deposits	Middle to late Permian	N12	Zhang et al. (2018a)
Akiyoshi Belt	Nishiki	Trench-fill and pelagic deposits	Middle to late Permian	N14	Zhang et al. (2018a)
Akiyoshi Belt	Nishiki	Trench-fill and pelagic deposits	Middle to late Permian	N16	Zhang et al. (2018a)
Akiyoshi Belt	Nishiki	Trench-fill and pelagic deposits	Middle to late Permian	N17	Zhang et al. (2018a)
Akiyoshi Belt	Itoigawa	Trench-fill and pelagic deposits	Middle Permian	A2	This study
Akiyoshi Belt	Itoigawa	Trench-fill and pelagic deposits	Middle Permian	A9	This study
Akiyoshi Belt	Itoigawa	Trench-fill and pelagic deposits	Middle Permian	B0	This study
Akiyoshi Belt	Itoigawa	Trench-fill and pelagic deposits	Middle Permian	B1	This study
Akiyoshi Belt	Itoigawa	Trench-fill and pelagic deposits	Middle Permian	B9	This study
Akiyoshi Belt	Itoigawa	Trench-fill and pelagic deposits	Middle Permian	C1	This study
Akiyoshi Belt	Itoigawa	Trench-fill and pelagic deposits	Middle Permian	C2	This study
Akiyoshi Belt	Itoigawa	Trench-fill and pelagic deposits	Middle Permian	C3	This study
Maizuru Belt	Tsuwano	Back-arc basin deposits	Middle Permian	TWN-SS01	Kimura et al. (2021)
Maizuru Belt	Itoigawa	Back-arc basin deposits	Middle Permian	190803-01	Ohkawa et al. (2022)
Maizuru Belt	Itoigawa	Back-arc basin deposits	Middle Permian	180502-05	Ohkawa et al. (2022)
Maizuru Belt	Itoigawa	Back-arc basin deposits	Middle Permian	190803-03	Ohkawa et al. (2022)
Maizuru Belt	Itoigawa	Back-arc basin deposits	Middle Permian	190803-04	Ohkawa et al. (2022)

Table 2 Summary of statistical values of morphologies for detrital zircons from Permian fore- and back-arc deposits, Itoigawa area (Ohkawa et al., 2022; this study). STD: standard deviation.

Fore-arc deposits

A2

	Width (µm)	Length (µm)	Elongation	Roundness
Count	109	109	109	109
Mean	69.0	98.6	0.72	4.0
STD	17.0	26.3	0.15	1.9
Min	41.0	59.0	0.37	1.0
25th percentile	55.0	79.0	0.61	3.0
50th percentile	67.0	94.0	0.72	4.0
75th percentile	77.0	112.0	0.82	5.0
Max	117.0	213.0	0.97	9.0

B9

	Width (µm)	Length (µm)	Elongation	Roundness
Count	102	102	102	102
Mean	56.1	83.7	0.69	4.4
STD	14.1	18.4	0.15	1.9
Min	35.0	41.0	0.33	1.0
25th percentile	48.3	71.3	0.57	3.0
50th percentile	53.0	82.0	0.69	4.0
75th percentile	61.8	95.8	0.79	5.0
Max	144.0	156.0	1.00	10.0

A9

	Width (µm)	Length (µm)	Elongation	Roundness
Count	101	101	101	101
Mean	68.5	97.7	0.72	3.8
STD	19.8	31.8	0.13	1.6
Min	36.0	49.0	0.33	1.0
25th percentile	54.0	81.0	0.62	3.0
50th percentile	67.0	91.0	0.71	4.0
75th percentile	80.0	107.0	0.82	5.0
Max	151.0	254.0	0.99	8.0

C1

	Width (µm)	Length (µm)	Elongation	Roundness
Count	109	109	109	109
Mean	61.8	87.8	0.72	4.4
STD	15.0	19.3	0.14	1.9
Min	34.0	38.0	0.41	1.0
25th percentile	51.0	76.0	0.61	3.0
50th percentile	60.0	86.0	0.72	4.0
75th percentile	71.0	99.0	0.82	5.0
Max	128.0	142.0	0.98	10.0

B0

	Width (µm)	Length (µm)	Elongation	Roundness
Count	169	169	169	169
Mean	57.7	86.2	0.69	4.4
STD	13.2	20.0	0.15	1.8
Min	34.0	44.0	0.35	1.0
25th percentile	48.0	71.0	0.57	3.0
50th percentile	55.0	86.0	0.70	4.0
75th percentile	65.0	100.0	0.79	5.0
Max	121.0	142.0	0.99	10.0

C2

	Width (µm)	Length (µm)	Elongation	Roundness
Count	109	109	109	109
Mean	56.9	82.8	0.70	4.4
STD	11.2	16.6	0.14	1.8
Min	34.0	42.0	0.43	1.0
25th percentile	49.0	71.0	0.59	3.0
50th percentile	57.0	81.0	0.70	4.0
75th percentile	63.0	94.0	0.81	6.0
Max	90.0	133.0	0.98	8.0

B1

	Width (µm)	Length (µm)	Elongation	Roundness
Count	100	100	100	100
Mean	62.0	85.9	0.73	3.9
STD	12.3	16.6	0.12	1.8
Min	34.0	49.0	0.46	1.0
25th percentile	53.8	76.0	0.64	2.8
50th percentile	61.0	85.0	0.74	4.0
75th percentile	68.0	93.3	0.81	5.0
Max	95.0	131.0	0.99	9.0

C3

	Width (µm)	Length (µm)	Elongation	Roundness
Count	110	110	110	110
Mean	64.6	89.6	0.73	4.4
STD	14.4	20.8	0.13	1.8
Min	35.0	43.0	0.38	1.0
25th percentile	54.0	76.0	0.66	3.0
50th percentile	64.0	88.0	0.73	4.0
75th percentile	73.0	100.0	0.85	6.0
Max	116.0	154.0	0.97	9.0

Back-arc deposits

190803-01

	Width (µm)	Length (µm)	Elongation	Roundness
Count	91	91	91	91
Mean	74.5	110.4	0.69	6.3
STD	18.4	26.3	0.15	2.0
Min	37.0	57.0	0.42	2.0
25th percentile	61.0	94.0	0.58	5.0
50th percentile	71.0	106.0	0.68	7.0
75th percentile	87.5	129.5	0.80	8.0
Max	122.0	171.0	0.98	10.0

180502-05

	Width (µm)	Length (µm)	Elongation	Roundness
Count	121	121	121	121
Mean	62.1	92.8	0.69	6.1
STD	13.5	21.9	0.12	1.8
Min	41.0	48.0	0.42	2.0
25th percentile	52.0	75.0	0.59	5.0
50th percentile	59.0	91.0	0.69	6.0
75th percentile	68.0	111.0	0.78	7.0
Max	109.0	151.0	0.96	10.0

190803-03

	Width (µm)	Length (µm)	Elongation	Roundness
Count	110	110	110	110
Mean	59.9	104.1	0.61	3.4
STD	14.0	33.6	0.16	1.6
Min	35.0	40.0	0.25	1.0
25th percentile	51.0	81.0	0.49	2.0
50th percentile	57.5	96.5	0.60	3.0
75th percentile	69.0	125.0	0.72	4.0
Max	98.0	217.0	0.97	9.0

190803-04

	Width (µm)	Length (µm)	Elongation	Roundness
Count	104	104	104	104
Mean	59.3	106.3	0.58	3.1
STD	15.5	31.5	0.13	1.3
Min	33.0	54.0	0.29	1.0
25th percentile	48.8	87.0	0.49	2.0
50th percentile	55.0	100.0	0.56	3.0
75th percentile	67.3	118.5	0.66	4.0
Max	137.0	211.0	0.90	7.0